# Water Structure from Scattering Experiments and Simulation

Teresa Head-Gordon*

*Department of Bioengineering, University of California at Berkeley, and Physical Biosciences Division, Lawrence Berkeley National Laboratory, Berkeley, California 94720*

Greg Hura

*Graduate Group in Biophysics, University of California at Berkeley, and Physical Biosciences Division, Lawrence Berkeley National Laboratory, Berkeley, California 94720*

## Contents

## 1. Introduction

Given the importance of water and its well-discussed anomalies, there are a large number of monographs,[1-4] reviews,[5,6] and even popular literature[7] that cover a much broader range of water topics than our focus on water structure. The seven volume series on water edited by Felix Franks sets the standard for comprehensive coverage of this arguably most important liquid.[1] Nonetheless, water structure is a vital component of our understanding of processes in water including the origin of its peculiar properties,[8,9] phase changes,[10] treatment of orientational effects,[11,12] hydrophobic hydration,[13-18] hydrogen bonding,[19-21] the benchmarking of water models,[22-34] and emerging ab initio simulation methodologies.[35-38] This review presents the progress of the experimental scattering and simulation fields into the 21st century in the structural characterization of liquid water.

This progress is measured in part by the reliability and reproducibility of the experimental data and analysis obtained for water structure under various conditions. We are especially attentive to the issue raised by Karnicky and Pings in their 1976 review of the X-ray diffraction of liquids[39] that "there are many possible sources of systematic error in the quite intricate process of going from experimental count rate to the distribution functions which describe the liquid structure". We therefore devote considerable space in this review to the procedures of scattering data acquisition, data reduction, and analysis in X-ray and neutron scattering. At the same time this exposure allows for appreciation of the fundamental difficulties of these experiments and the important progress made by the experimental community over the last 25 years to improve the quality of scattering data on liquid water, not only under ambient conditions as recently reported by our own group,[40,41] but in different thermodynamic regimes such as supercooled[42-45] or supercritical,[46-50] in confined geometries,[51] or in aqueous solutions of biochemical or chemical importance.[13,23,52-59]

This review also measures the progress in the simulation of liquid water structure. It is important to emphasize that the quality of a water model or simulation should be judged more broadly than the structure it produces, such as its performance for thermodynamic or phase stability properties, or to consider the intended purpose of the model to decide if more severe approximations are warranted. Given the scope of this review, we will focus exclusively on the structural properties obtained by the various theoretical modeling approaches, with the understanding that one water model or approach is not to be preferred over others based *solely* on better structural performance. When we consider the characterization of water structure over the liquid region of the phase diagram, it is apparent that computer simulation has played an equal, and sometimes pivotal, role with respect to experiment in both the quantitative characterization of the water liquid and the advancement of our qualitative understanding of water and its anomalies.

## 2. Liquid Water Structure

The fundamental unit of water structure is the hydrogen bond. In ice I a given water molecule is hydrogen bonded to four water neighbors in a tetra-

* To whom correspondence should be addressed.

Teresa Head-Gordon was born in Ohio in 1960. She received her B.S. degree in Chemistry at Case Western Reserve University in 1983. After waitressing for over a year, she eagerly took up her Ph.D. studies at Carnegie Mellon University, receiving her Ph.D. degree in Theoretical Chemistry in 1989 under the direction of Charles L. Brooks III. From 1990 to 1992 she was a Postdoctoral Member of the Technical Staff at Bell Laboratories working with Dr. Frank Stillinger on protein folding and perturbation theories of water. She then took up a staff scientist position at Lawrence Berkeley National Laboratory (LBNL) from 1992 to 2001. She now is an assistant professor in the Department of Bioengineering at UC Berkeley, a faculty staff scientist at LBNL, a member of UC Berkeley's graduate groups in Bioengineering, Biophysics, and Applied Sciences and Technology, and Department Head of the Computational Structure Group in the Physical Biosciences Division at LBNL. She has published over 50 papers in the areas of theoretical, computational, and experimental biology and chemistry.
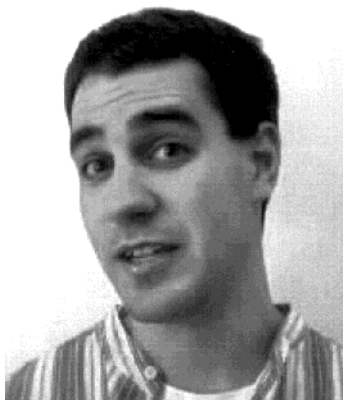
Greg Hura was born in New York City in 1973. He received his B.A. degree in Physics from UC Berkeley in 1996. He is currently a graduate student in the Biophysics Graduate Group at UC Berkeley under the guidance of Teresa Head-Gordon. His thesis project is on the effects of hydration in protein folding using solution scattering experiments. In his free time he enjoys hiking the Sierras of California.

hedral structure that gives rise to a crystal made up of connected hexagonal rings. In the case of crystalline materials such as ice I, X-rays and neutrons are scattered by atomic centers at discrete angles represented as sinusoidal (Fourier) components of the electron density and nuclear scattering potential of the specimen, respectively. The scattering angle, $\theta$, is determined by the spatial period of the Fourier component that is responsible for the scattering; thus, for each scattering angle there is a corresponding Bragg spacing, $d$, which is given by

$$d = \frac{\lambda}{2 \sin(\theta/2)} = \frac{2\pi}{Q} \quad (1)$$

where $\lambda$ is the radiation wavelength and $Q$ is the momentum transfer. The spatial period of each Fourier component of the electron density is determined by the lengths of the unit cell vectors of the crystal. In the case of normal ice for which the solid is made up of hydrogen-bonded hexagons, the largest Bragg spacing observed with X-rays is ~0.39 nm. Cubic ice is also composed exclusively of hydrogen-bonded hexagons, but in this case the largest Bragg spacing is 0.37 nm.[42,60]

Representation of the electron density as a sum of Fourier components is equally applicable to noncrystalline materials, however, such as the water liquid. As a result it is still true that the spatial period of the Fourier component, which we can call an effective Bragg spacing, can be calculated from the measured scattering angle according to the above equation. As with crystalline materials, the amplitude of each Fourier component of the electron density is given by the square root of the scattered intensity. Information about the vector direction of the Fourier component is lost in scattering from liquids, however, unlike the case of crystals.

In the case of liquid water, the strict adherence to hydrogen-bonded hexagons of the ice crystal gives way to greater translational and rotational motion of waters and a broader distribution of hydrogen-bonded configurations, including a variety of polygons of varying sizes and degrees of puckering or distortion, all of which result in a more compact arrangement of water molecules. The electron density of the liquid is now characterized by the scattering as a diffuse water ring rather than a discrete distribution of Fourier components, and the effective Bragg spacing associated with the main water peak is found to be ~0.31 nm.

Furthermore, the scattering intensity is peaked at a distance that remains larger than the center-to-center distance between individual water molecules, which is typically ~0.28 nm. Thus, it is clear that the most prominent Fourier components of the scattering density of pure liquid water have a repeat distance that is larger than the oxygen–oxygen nearest neighbor distance. The larger Bragg spacing tells us that the fundamental scattering unit in liquid water must be something bigger than pairs of hydrogen-bonded water molecules. In fact, it is a measure of the highly associated three-dimensional hydrogen-bonded *network* of the water liquid. The importance of accurate experimental information and classical and emerging ab initio simulation methodologies is their ability to characterize this fundamental unit of scattering to help us to understand the topology of the hydrogen-bonded network over the full phase diagram.

## 3. Diffraction Principles of X-ray and Neutron Scattering

Water structure is primarily determined experimentally from X-ray[39,40,49,61−68] and neutron scattering.[9,42,45,69−75] Scattering experiments probe the differential scattering cross-section,[76] $d\sigma/d\Omega$, defined as the ratio of the scattering cross-section $d\sigma$ scattered into the solid angle $d\Omega$ about the scattering

angle $\theta$.[76] This can be analyzed in terms of the first Born approximation[76]

$$I(Q) = \frac{d\sigma}{d\Omega} = \left\langle \sum_{i,j}^{N} b_i b_j \exp(i\mathbf{Q}\cdot\mathbf{r}_{ij}) \right\rangle \qquad (2)$$

where the sums are over the $N$ nuclei (in the case of neutrons) or electrons (in the case of X-rays) in the sample, $b$ is the scattering length for neutrons of a given element, while $b$ is replaced by a $Q$-dependent form factor in the case of X-rays; the $\{\mathbf{r}_{ij}\}$ are the positions of the nuclei or electrons; $\mathbf{Q} = 4\pi sin(\theta/2)/\lambda$ is the momentum transfer for the elastic scattering process where $\lambda$ is the wavelength, and the brackets correspond to a thermal average in eq 2. In applying this formula it is required that various corrections to the experimental data have been made, accounting for effects such as incoherent scattering, beam polarization, multiple scattering, inelastic effects, container absorption, etc., which we return to in section 4.

The fundamental difference between neutron and X-ray scattering is the mechanism by which the incident radiation interacts with the material, which in turn leads to several important differences in how the experimental data is obtained and corrected. X-rays are scattered by the electron density of an atom or molecule, and the scattering cross-section of an atom increases in direct proportion to the square of the number of electrons or atomic number, Z; in the case of water or ice the X-rays "see" the electron clouds contributed by oxygen's eight electrons better than the single electron attributable to hydrogen. X-rays probe atomic dimensions within an order of magnitude of the X-ray wavelengths, so that the radiation scattered by the electron cloud on opposite sides of the atom results in a different path length that gives rise to a shift in phase and decreasing the scattering power with increasing scattering angle.[77] Because X-rays probe the distribution of electrons, the scattering is usually not spherically symmetric in molecularly interesting materials and the redistribution of charge upon chemical bonding or polarization in the condensed phase can effectively decrease or increase the effective atomic number, making the analysis of the experimental data more challenging, which is the case for liquid water as we shall see later.[41,78]

Neutrons interact directly with the nuclei within a molecule, and the strength of the scattering interaction varies irregularly with atomic number, so that even isotopes of the same element do not have the same neutron scattering cross-section or scattering length.[79] For example, the most significant isotopic variation occurs for hydrogen, which has a coherent scattering length of $-3.74$ fm, while for deuterium the scattering length is 6.67 fm. Neutrons are therefore sensitive to hydrogen and differences between its isotopes, which permits observation and measurement of the hydrogen structural correlations in water that are not easily obtainable by X-rays.

X-ray photons have typical wavelengths of $0.5-1.8$ Å and are most typically generated by conventional anode generators that offer the advantage of in-house capabilities found in individual laboratories worldwide, as well as the bright light of synchrotron sources that are available only at national facilities. The flux of photons produced by X-ray synchrotrons is several orders of magnitude higher than the flux on a neutron beamline. The increased flux can be very beneficial when collimating the beam to a spot size of few millimeters in diameter and for increasing the experimental throughput based on reduced exposure time needed. $Q$-ranges covered are typically $0.3$ Å$^{-1}$ $< Q < \sim 15$ Å$^{-1}$ in typical water diffraction experiments.

The various diffractometers used in neutron scattering rely on either reactors or spallation sources for neutrons.[80,81] Reactor sources are continuous and typically select neutrons of a specific wavelength from the beam using a monochromator. Spallation sources have higher intensity neutrons than reactor sources, and the neutrons exhibit a range of wavelengths. $Q$-ranges covered for reactors that use monochromators are similar to those of X-ray, while spallation sources cover a wide $Q$-range of approximately 0.5 Å$^{-1}$ $< Q < 35-50$ Å$^{-1}$.

The scattered radiation signal is captured by a detector, or detector element, of dimensions $dx \times dy$ positioned at some distance, $L$, and scattering angle from the sample and records the flux of radiation scattered into a solid angle element, $d\Omega = dxdy/L^2$. Single-point detectors have been used to collect X-ray structural information from water, but area detectors offer several important advantages over single-point detectors, including reduction of background signal and greater statistics, a larger range of $Q$-space data collected at the same time, and the collection of several perspectives of the same data that provides an important benchmark for validation of the subsequent data processing. The use of charge-coupled device (CCD) area detectors for X-ray diffraction began around 1995 and has become increasingly popular.[82-84] Commonly available CCD detectors are typically flat and require geometric corrections to the data to account for the variations in the radius; we return to these corrections later in this section.

The detection of neutrons is typically accomplished through an array of individual detectors (although one- and two-dimensional linear and area detectors are sometimes used) composed of a gas of $^3$He, for example, or scintillator materials based on $^6$Li that detect the neutron as a charge produced from a nuclear reaction.[81] The primary issues in devising a neutron detector is to create high sensitivity to neutrons while remaining insensitive to background events (such as $\gamma$-rays) and to minimize the loss of signal due to the "dead-time" of the detector. Gas detectors have the advantage of good discrimination against $\gamma$-rays, while scintillator detectors have better sensitivity relative to gas detectors, with a dead time on the order of hundreds of nanoseconds, and both realize good insensitivity to $\gamma$-rays.[81,85]

## 4. Data Analysis Procedures in Experimental Scattering

### 4.1. X-ray Scattering

It is conventional in the analysis of the X-ray scattering from molecular liquids to further separate eq 2 into contributions from individual molecules (self-scattering), also known as the molecular form factor or $\langle F(Q)^2\rangle$, and that arising from intermolecular correlations, $S(Q)$. In the case of X-rays the assumption is commonly made that the scattering can be represented as arising from independent neutral atoms, each with a spherical electron density distribution. Within this approximation, the experimental intensity is now defined as

$$I(Q) = \sum_{ij} x_i x_j f_i(Q) f_j(Q) \frac{\sin Qr_{ij}}{Qr_{ij}} + \sum_{i \le j} x_i x_j f_i(Q) f_j(Q) S_{ij}(Q) \quad (3)$$

where $x_i$ is the atomic fraction of atom type $i$, $f_i(Q)$ is the $Q$-dependent atomic scattering factor[22] for atom type $i$, and $r_{ij}$ is the intramolecular distance between atom centers. The intermolecular correlations are determined by the Fourier transform relation

$$S_{ij}(Q) = 1 + 4\pi\rho \int_0^\infty r^2 dr [g_{ij}(r) - 1]\frac{\sin Qr}{Qr} \quad (4)$$

where $\rho$ is the atomic number density and $g_{ij}(r)$ is a partial radial distribution function between atom types $i$ and $j$. The partial structure factors, $S_{ij}(Q)$ are the most fundamental aspect of structure of the hydrogen-bonded network in water that we can determine directly from scattering experiments.

In any scattering experiment, several corrections must be applied to the raw data image in order to report a meaningful intensity that can be compared to other experiments and from which radial distribution functions can then be extracted. Part of the raw collected intensity is unwanted scattering from the sample container or windows, scattering by air or helium in the path length of the beam, as well as spurious peaks that arise from backscattering from the lead beam stop. The sample holder and air scattering are usually removed by measuring the intensity with an empty sample holder that is then subtracted from the intensity recorded after the sample holder had been filled, while the sharp backscattering peaks may be manually removed.

Because the intensity of the scattered radiation experiences a $1/a^2$ falloff before reaching the detector and being recorded and the geometric position of individual pixels of a flat plane area detector are at different values $a_i$ from the sample, X-ray data is further corrected by multiplying a given pixel's intensity by $a_i^2$ based on careful measurement of the sample and detector geometry. Additionally, pixels may not be oriented perpendicular to the incident X-rays they collect, so that an additional data processing step is required that amplifies the intensity based on the dot product of the incoming intensity vector and the normal vector to the face of the pixel. Furthermore, because all pixels are not equally sensitive, each pixel's relative sensitivity is calibrated by what is often referred to as the flat field correction. It is important to know what type of flat field correction is being used by the detector software in the processing of image read-out since the radial dependence of radiation falloff and pixel orientation that must be applied to flat area detectors may be *partially* taken into account by the manufacturer in the flat field correction.

In X-ray scattering we must correct the raw intensity for radiation that is absorbed by the sample and which never reaches the detector. The absorption of X-rays (and neutrons) follows Beer's Law and has the generic form

$$I = I_0 \exp(-\mu_\rho t) \quad (5)$$

where $I_0$ is the intensity if there were no absorption in the sample, $I$ is the measured intensity, $\mu_p$ is the product of the X-ray absorption coefficient and the density of the water sample, and $t$ is the sample thickness. Further geometric factors must be considered when the incident beam is at an angle to the sample as well as the fact that the absorption event can occur along the effective path length, $t$, a variable that must be integrated over. For example, using a transmission geometry for a flat slab sample tilted at an angle $\tau$ between the plane of sample and the incident X-ray beam, the absorption correction was of the form[40]

$$\frac{I}{I_0} = \left[\exp\left(\frac{-\mu_\rho t}{\sin \tau}\right) - \exp\left(\frac{-\mu_\rho t}{v}\right)\frac{v \sin \tau}{\mu_\rho(\sin \tau - v)}\right] \quad (6)$$

where $v = \cos \theta \sin \tau + \sin \theta \cos \phi \cos \tau$. Similarly, neutron scattering also has a number of functional forms for the absorption correction that are dependent on the sample geometry, which are well described in ref 81.

The raw scattering data also requires a correction due to the polarization of the source.[86] If the incident radiation is unpolarized (random orientation of the electric vector of the radiation), as is common for rotating anode sources, then the polarization correction is given by

$$P = \frac{1}{2}(1 + \cos^2 \theta) \quad (7)$$

When the incident radiation is polarized (such as the synchrotron X-ray experiment reported in ref 40), the in-plane and out-of-plane polarization is treated separately and the measured intensities must be rescaled by the factor

$$P = P_{\text{in-plane}}[1 - (\sin \phi \sin \theta)^2] + P_{\text{out-plane}}[1 - (\cos \phi \sin \theta)^2] \quad (8)$$

where $P_{\text{in-plane}}$ and $P_{\text{out-plane}}$ are the fractional polarizations of the beam in the plane and out of the plane of the circulating electrons, respectively.

True structural information is only contained in coherent, single scattering events. The effect of multiple scattering, with double scattering as the leading term, must be corrected when thick or dense samples are used. Bright X-ray synchrotron sources now permit the use of very thin water samples, so that secondary scattering events are not a significant problem. They are also not a problem because the X-ray absorption cross-section is large compared to the scattering cross-section. An estimate of the ratio of multiple scattering[87] to primary scattering is less than 1% for samples with $\mu_p t \approx 0.1$ in the case of X-ray scattering. With neutrons the ratio of capture to scattering cross-section is much smaller, so there is a much greater chance multiple scattering can occur. Monte Carlo simulations are used to determine the ratio of primary to secondary scattering probabilities.

In the case of X-rays, one of the two greatest sources of systematic error is due to radiation that is incoherently scattered or the Compton effect. Only coherently scattered radiation carries any intermolecular structural information about the sample, with the incoherent scattering carrying only information about the atoms acting alone (i.e., no diffraction). Incoherent scattering manifests itself as a $Q$-dependent signal in the case of Compton scattering. Using conservation of energy and conservation of momentum and the Planck relationship and relativistic energy expression, the following standard Compton formula is derived[88]

$$\lambda_f = \lambda_i + \frac{h}{m_e c}(1 - \cos\theta) \qquad (9)$$

More complicated functional forms of the Compton scattering correction will depend on whether the X-ray experiment is conducted with an energy dispersion technique.

Theoretical estimates for the Compton scattering corrections use inelastic scattering intensities derived from wave functions calculated with Hartree−Fock and minimal basis sets[89] and with electron correlation using both the CISD and CCSD levels of theory and basis sets that include polarization and diffuse functions.[90,91] The Compton scattering calculations using CISD and CCSD theories agree accurately with incoherent scattering from experiment on water.[92] Fitted Compton scattering curves to the CISD calculations are available for water and are therefore accurate for removal of the unwanted Compton scattering from the total measured intensity.

A second source of systematic error in X-ray scattering is the commonly made assumption of the Debye approximation (eq 3) that the scattering can be represented as arising from independent neutral atoms, each with a spherical electron density distribution.[93] However, approximating the electron density distribution of water as a superposition of electron densities centered on the individual atoms is unlikely to be representative of the true charge distribution.

Figure 1 shows the molecular form factor, $\langle F(Q)^2 \rangle$, for the gas-phase water monomer based on the Debye independent atom approximation with that derived
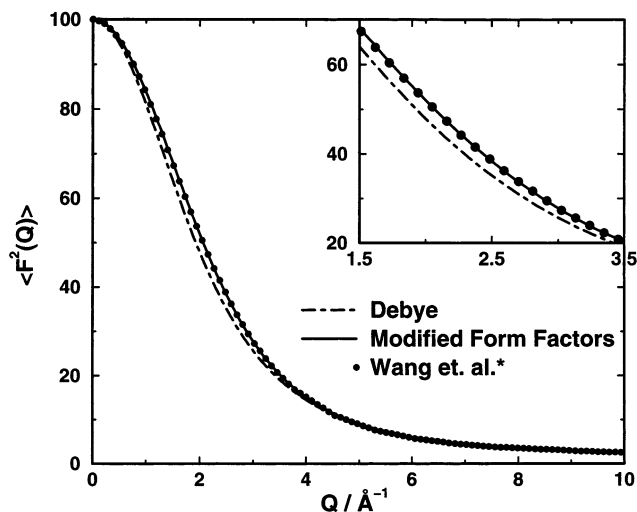


**Figure 1.** Molecular form factor, $\langle F(Q)^2 \rangle$, for water in the gas-phase. Legend: Debye independent atom approximation[93] (dot−dash line); Debye with modified atomic scattering factors (solid line);[41] four-Gaussian fit to CI calculation[90] (circles).

from electronic structure calculations;[90,94,95] the CI theoretical results reproduce the experimentally determined molecular form factor from recent X-ray scattering studies of gas-phase water after subtraction of incoherent scattering.[67] The Debye approximation in the region of $1.0{-}4.0$ Å$^{-1}$ differs significantly from the CI results. Unfortunately, this corresponds to the region of most interest for extracting the intermolecular correlations of water.

While we can state with certainty what is $\langle F(Q)^2 \rangle$ for the water monomer in the gas phase, the intramolecular term in eq 3 should correspond to the electron distribution around the water monomer in the condensed phase. We know that the charge distribution changes significantly from the gas phase to the liquid based on the observed gas-phase dipole moment of 1.85 D,[96] while it is estimated to increase to $2.6{-}3.0$ D in the liquid phase.[36] This change in dipole reflects that the water molecule in the condensed phase is much better represented as having far more charge around the oxygen atom than is the case for the isolated atom. The Debye approximation has the effect of overly weighting the hydrogen correlations and further obscuring whether a simulated or extracted $g(r)$ corresponds to reality.

Deviations from the independent atom model due to chemical bonding effects have been known and studied for many years in the small molecule X-ray diffraction literature[78,97,98] and more recently in solution scattering,[41,57] and in the context of appropriate form factors for electron crystallography.[99,100] We have recently introduced a modification of the atomic scattering factors for liquid water which rescales them properly at low $Q$ where chemical bonding effects are known to be significant while retaining their values at large $Q$ where chemical bonding effects on the core electron distribution should be negligible.[41] The modified atomic scattering factor (MASF) $f'(Q)$ is of the form

$$f'(Q) = [1 + (\alpha - 1)\exp(-Q^2/2\delta^2)]f(Q) \qquad (10)$$

where $f(Q)$ is the atomic scattering factor for the isolated atom, $\alpha$ is a scaling factor giving the redistribution of charge, and $\delta$ is a parameter to be fit, representing the extent of valence-electron delocalization induced by chemical bonding. For gas-phase water, we choose $\alpha$ to correspond to the gas-phase dipole moment, while for liquid water, we choose $\alpha$ to correspond to the condensed phase dipole moment of 2.8 D; the unknown parameter $\delta$ was fit by requiring the Debye expression curve to agree with the ab initio CI results for gas-phase water.[41] Figure 1 shows that the Debye expression using the modified atomic form factors agrees excellently with the CI results. The advantage of the MASF formalism lies in the firmer foundation it provides for extraction of the oxygen−oxygen (OO) and possibly oxygen−hydrogen (OH) correlations from the experimental scattering curves. With the proper scaling, they allow the correct weighting of OO and OH correlations, allowing one to extract $g_{OO}(r)$, i.e., the internuclear distances, and not only a molecular centers radial distribution function.

## 4.2. Neutron Scattering

In neutron scattering, we also work with eq 1 but it is now more useful to consider the differential scattering cross-section in terms of self- and distinct scattering[101]

$$\frac{d\sigma}{d\Omega} = \left(\frac{d\sigma}{d\Omega}\right)^{self} + \left(\frac{d\sigma}{d\Omega}\right)^{distinct} \quad (11)$$

As is the case for X-rays, no diffraction information about the sample is contained in the incoherent scattering. The advantage of this division of the scattering cross-section is to isolate the unwanted effect of incoherent scattering into the self-scattering term.

$$\left(\frac{d\sigma}{d\Omega}\right)^{self} = (b_O{}^2 + b_D{}^2) + 2\frac{\sigma_D{}^{incoherent}}{4\pi} \quad (12)$$

The contribution of incoherent scattering comes from either hydrogen or deuterium, since the incoherent cross-section of oxygen is zero. Since the incoherent scattering cross-section of hydrogen is extremely large, many neutron scattering experiments focus on $D_2O$ instead.

The distinct part of the scattering has contributions from both intermolecular and intramolecular scattering

$$\left(\frac{d\sigma}{d\Omega}\right)^{distinct} = \left(\frac{d\sigma}{d\Omega}\right)^{intermolecular} + \left(\frac{d\sigma}{d\Omega}\right)^{intramolecular} \quad (13)$$

The water liquid scattering factor, $S(Q)$, is directly related to the distinct scattering term

$$S(Q) = \frac{\left[\left(\frac{d\sigma}{d\Omega}\right)^{distinct} + (b_O{}^2 + 2b_D{}^2)\right]}{(b_O{}^2 + 2b_D{}^2)^2} \quad (14)$$

which can be rewritten in terms of the molecular form factor, $\langle F(Q)^2\rangle$, and a scattering function, $D_M(Q)$, that contains all of the intermolecular correlations

$$S(Q) = D_M(Q) + \langle F(Q)^2\rangle \quad (15)$$

A pair correlation function, $g_L(r)$ can be determined by Fourier transform of $D_M(Q)$

$$4\pi r \rho_M(g_L(r) - 1) = \frac{2}{\pi}\int_0^\infty Q D_M(Q)\sin(Qr)\,dQ \quad (16)$$

where $\rho_M$ is the molecular density and $g_L(r)$ is composed of the following weighted contributions from the partial pair correlation functions (with the coefficients relevant only for $D_2O$)

$$g_L(r) = 0.489 g_{DD}(r) + 0.421 g_{OD}(r) + 0.090 g_{OO}(r) \quad (17)$$

This result indicates that the signal is dominated by D−D and O−D correlations, although the resulting $r$-space quantity cannot separate out these two site−site correlation functions directly.

The technique of isotopic substitution pioneered by Enderby[52] and since used by other groups[55,73] has provided a new approach for obtaining all three site−site correlation functions for liquid water. By performing three measurements on pure $H_2O$, pure $D_2O$, and a mixture of $H_2O$ and $D_2O$, we can exploit the scattering contrast of hydrogen and deuterium to isolate the three site−site correlation functions directly.[52] The primary problem with this approach is the large uncertainty in the inelasticity correction when all three correlation functions are extracted from the intensity scattering data.[102,103]

For water the inelastic scattering is a background signal that is weakly dependent on $Q$ and is primarily contained in the self-scattering term. It has been shown elsewhere[104] that the distinct part of the scattering is not strongly affected by inelasticity, but nonetheless $S(Q)$ cannot be isolated until an inelasticity-corrected self-scattering term is determined.[104,105] In principle, its subtraction should be straightforward and the remaining distinct scattering would isolate the desired radial distribution function(s). However, a problem arises in practice that the measurement is not performed at constant $Q$, but instead the cross-section is measured at constant scattering angle $\theta$. This measurement at constant $\theta$ means that the integrand of eq 16 is a different function, which now accounts for detector efficiency, incident and scattered flight paths, and incident neutron spectrum energy. This different integration path also means that the inelastic scattering contained in the self-scattering term is no longer a simple $Q$-independent background signal, and therefore, the subtraction of self-scattering to isolate $S(Q)$ is very difficult.

Plazcek devised a correction to the inelasticity problem based on an expansion of the revised integrand to give the desired $S(Q)$ as the leading term.[106] Since the first few moments arise mostly from recoil effects, the "conventional" Plazcek approach is to correct for inelastic scattering using a mass expansion in powers of neutron mass to atomic mass instead whose first and second moments are analytically known. Because the Plazcek approach is only

viable for a rapidly convergent expansion in mass ratios of neutron to atomic mass (and the correction is more complicated for molecules where an effective mass is ill-defined), it is clearly less applicable to hydrogen-containing or low molecular weight materials such as water. Furthermore, the inelasticity corrections become more difficult for higher temperatures and low neutron energies as discussed in refs 102, 105, and 107.

Essentially the problem of inelasticity corrections to neutron data can only be solved numerically for water. For example, one approach discussed by Soper and Luzar is to estimate the self-scattering by a Chebyshev polynomial fit, made consistent with Krogh–Moe normalization (essentially the requirement that the radial distribution function $g(r)$ be zero below some minimum value of $r$) through a maximum entropy method.[108] Zetterstrom et al. parametrized the Van Hove dynamic self-scattering law,[105,107] while more recently the removal of inelasticity is attempted using the empirical potential structural refinement (ESPR) method.[109] Alternatively, Bellissent-Funel, Bosio, and Teixeira[110] fit the first few moments of the Placzek expansion by enforcing the condition that the Fourier transform of $S(Q)$ (eq 16) from their reactor data exhibits no density at low $r$, since the intramolecular scattering contributions have been removed from the scattering factor.

Before we can extract the radial distribution functions from the experimental intensities, we must place the intensities on an absolute scale. The Krogh–Moe[111] and Norman[112] methods are typically the approach used to normalize scattering data for X-rays. These so-called integral methods find the scale factor $\beta$ required to put the data on an absolute scale with intensity in appropriate units, which uses the fact that as $r$ goes to zero, $g(r)$ goes to zero. In the case of X-ray data, the scale factor $\beta$ is given as

$$\beta = \frac{-2\pi^2 z^2 \rho + \int_0^{Q_0} Q^2 [f^2(Q) + I_{\text{incoherent}}(Q)]\,\mathrm{d}Q}{\int_0^{Q_0} Q^2 I_{\text{experiment}}(Q)\,\mathrm{d}Q} \tag{18}$$

where $\rho$ is the molecular density (in molecules/Å³), $z$ is the number of electrons per water molecule, $Q_0$ is the maximum value of momentum transfer available in the experiment, $f(Q)$ is the water molecule molecular form factor, $I_{\text{incoherent}}(Q)$ is the incoherent or Compton scattering from the sample, and $I_{\text{experiment}}(Q)$ is the experimental curve to be normalized. Alternatively, for data that is available at very large $Q$, the experimental intensity should match the structureless free atom intensity

$$I(Q) = \beta f^2(Q)|_{\text{high}\,Q} \tag{19}$$

While in principle these methods should give the same absolute scale, it has been stated that the integral methods are more accurate since they use the whole of the experimental intensity curve.[39] In the case of neutron scattering, the use of eq 18 or 19 is avoided by using a vanadium sample to calibrate the detectors for efficiency and solid angle and to put the data on an absolute scale.

## 4.3. Extracting Radial Distribution Functions from Scattering Data

Straightforward application of eqs 2–4 to extract the $g(r)$'s for water from the $S(Q)$'s is not possible due to the errors introduced by experimental truncation in $Q$-space. The apparent exception to this is the composite $g_L(r)$ defined in eq 17 that is formulated to avoid truncation errors.[110] Otherwise, the $g_{OO}(r)$ obtained from such a procedure has spurious peaks introduced by the truncation and does not display the proper limiting behavior at small $r$.[62,66]

One possible approach for avoiding these truncation errors for extracting $g(r)$'s is to use a $Q$-space continuation method[113] in which the experimentally truncated $Q$-space is extended to infinity based on the analysis that the first coordination shell in water is more cleanly separable in $Q$-space than $r$-space and in fact dominates the scattering correlations beyond $7-9$ Å$^{-1}$.[41,66,113] A Gaussian function is used to describe this first-shell coordination in $r$-space

$$\Gamma(r) = \frac{\alpha}{\sqrt{4\pi\gamma}}\exp\!\left(\frac{-(r - r_{\text{max}})^2}{4\gamma}\right) \tag{20}$$

where $\alpha$, the area under the Gaussian, $r_{\text{max}}$, the position of the maximum in the first peak, and $\gamma$, related to the width of the Gaussian, are parameters that are fit to the tail of the scattering data at the largest available values of $Q$.[66,113] The radial distribution function of molecular centers is then given by

$$4\pi r \rho g(r) = \Gamma(r) + 4\pi r\rho + \frac{1}{2\pi}\int_0^{Q_{\text{max}}}[Qi(Q) - y(Q)]\sin(Qr)\,\mathrm{d}Q \tag{21a}$$

where

$$y(Q) = \alpha\exp(-\gamma s^2)\sin(Qr_{\text{max}}) \tag{21b}$$

which ensures that the difference function in the integrand of eq 21a goes to zero well before $Q_{\text{max}}$, thereby avoiding termination ripples in the extracted $g(r)$'s.[66,113]

Our group recently introduced a procedure that differs from the above approaches in that we proceeded from combinations of real-space functions to find the optimal $g_{OO}(r)$ which best fit the experimental data.[41] The advantages of working in real space while fitting the experimental curve is that we remain the entire time in a space of functions that satisfy the important small-$r$ and global constraints on possible $g_{OO}(r)$'s. Truncation errors in $Q$-space are no longer a problem, and we can address the issue of what range of RDF's will satisfy the data in the given experimental $Q$-range. However, truncation in $r$-space is now a possible problem, depending on how far our basis functions continue in real space. Fortunately, this only affects the low-$Q$ region of the predicted scattering curve, where the behavior of the pure water scattering curve at smaller angle is mostly uninteresting and simply describes the lack

of significant long-wavelength correlations in liquid water. The $Q = 0$ value of the scattering curve gives the isothermal compressibility of water and enforces a constraint on the total integral of the RDF's. However this constraint should be enforced only strictly at the $r = \infty$ limit of the RDF's and can only be used as an approximate constraint at finite values of $r$.

Reverse Monte Carlo (RMC)[114,115] was introduced by McGreevy and Puszati in 1988 to provide a more objective approach for constructing rdfs from real scattering data obtained on condensed phase disordered systems, with no reliance on a theoretical potential energy surface at a given thermodynamic point. In RMC, atom or molecule configurations are generated from a normal probability distribution of the difference between a calculated and experimental structure factor, whereas in Metropolis Monte Carlo the configurations generated follow a Boltzmann distribution of energies.

However, it appears that the experimental data alone is inadequate for generating physically sound molecular configurations. The underlying noise or truncation of the experimental data at high $Q$ make the region of zero density due to the excluded volume of atoms or molecules ill defined or unphysical. The corresponding three-dimensional structure of the liquid may also be poor, since the RMC approach assumes that the superposition approximation is valid. For liquids such as water, higher order correlations (angular correlations of hydrogen bonding, for example) can deviate significantly from the tetrahedral network that describes liquid water structure using RMC.

Although RMC was originally motivated to not rely on a model for the intermolecular potential, practical extensions of the RMC method require at least a geometrical model of the water molecule, some constraint that mimics the short-ranged repulsive behavior between molecules known to be vital determinant of fluid structure, and often a starting configuration that derives from a molecular simulation of water. An example of such a practical approach is to define constraints based on the experimental scattering data on an existing water model potential, such as Soper's empirical potential structural refinement (EPSR).[109] The reference potential is usually a simple model form, such as the SPC/E water potential, that acts between sites and added to this is a "potential of mean force" based on the best guess of the experimental radial distribution function

$$W_{\alpha\beta}(r) = -k_b T \ln[g_{\alpha\beta}(r)] \tag{22}$$

to give an effective potential

$$V_{\alpha\beta}(r) = V_{\alpha\beta}{}^{\text{ref}}(r) + k_b T \ln[g_{\alpha\beta}{}^{\text{Calc}}(r)/g_{\alpha\beta}{}^{\text{Expt}}(r)] \tag{23}$$

The effective potential is updated frequently after the particle moves until consistency in the potential is reached, after which statistics on the refined partial radial distribution functions can be collected. The use of a reference potential has helped avoid some of the artifacts of deriving unphysical $g(r)$'s from

the experimental data alone as well as overcome the problem of incomplete subtraction of the inelasticity error.[116] At the same time it has helped provide insight into the possible inadequacies of the reference potential itself and important feedback as to how simple model potentials can be improved in the future.

## 5. Classical and Quantum Simulations of Water Structure

We now turn to the theory and simulation of water structure. The allure of simulating water is that most if not all relevant structural, kinetic, and thermodynamic observables can be calculated at one time, in the context of a molecular model that provides insight and new hypotheses. At worst, simulation provides a venue for telling us what is not water-like or what physics is missing when calculated properties from the model disagree with the best experimental data sets available. Under the best of circumstances, when the numerical approximations are well understood or controlled and theory agrees well with experiment, simulation can provide a more global view of the versatility of the water fluid outside of the window of experimental observation.

A more comprehensive review of water models can be found in ref 117, and a review of modeling water under supercritical conditions can be found in ref 118. In this review we focus less on the specific models but more on the underlying modeling approach. Therefore, we consider an overview of modeling approaches starting with simple two-body empirical force fields originating from Rahman and Stillinger's realistic ST2 model, to more recent models that incorporate many-body effects through polarizability, and finally to first principles molecular dynamics studies based on well-defined approximations to the Schrödinger equation.

In the classical simulation arena, empirical water force fields have been developed for the neat liquid over the last several decades by fitting to liquid-state properties at ambient conditions. Some of the first simulation-based water models assume a rigid water geometry, with bond lengths close to 1 Å, bond angles somewhere between 104.5° and 109.5°, with the intermolecular potential typically composed of pairwise nonbonded interactions using Lennard–Jones 6–12 terms and Coulomb's Law for electrostatic interactions between atom sites.[22,24–27]

$$V_{ij} = \frac{q_i q_j}{r_{ij}} + 4\epsilon_{ij}\left[\left(\frac{\sigma_{ij}}{r_{ij}}\right)^{12} - \left(\frac{\sigma_{ij}}{r_{ij}}\right)^{6}\right] \tag{24}$$

The interaction between water molecules is the sum over all site interactions. It is not necessary that the interaction sites correspond to the atomic centers. There are important parametric variations based on eq 24 that may include attenuation of the point charge interactions based on the O–O distance as in the ST2 and ST4 models[11,22] or that the Lennard–Jones interaction is only carried by the oxygen centers for most all classical water potentials or even that the parametrization depends on use of a cutoff

based on radial separation of water molecules as in the TIP series of water models.[26,27] Rigid, fixed charge models can be viewed as "effective" potentials that inherently include quantum effects and electronic polarization through parametrized condensed phase values of the water dipole moment, for example. These models are still used routinely in the simulation of water properties but especially in biomolecular simulations where protein force fields are parametrized against these inexpensive and simple water descriptions.[119,120]

Polarizable empirical force fields were originally introduced by a number of groups starting in the late 1970s[121–123] to include many-body effects. Although they are also "effective" potentials, they treat the response of the electron density to an electric field or condensed phase environment in a more explicit way. It is thought that including polarizability into empirical force fields is necessary for improving the quantitative agreement between simulations and experiments away from ambient conditions, for dynamics, and for heterogeneous chemical systems.[28,124–126] They are typically fitted to properties of the liquid phase at ambient conditions and to properties of gas-phase monomers and clusters with the reasoning that fitting to two different thermodynamic states (with respect to density) should also yield a good description for other densities.[31]

Effective simulation strategies for including polarization were originally based on induced dipoles[127,128] that describes the local density distortions or response around a given atom, and the water liquid was one of the first systems in which parametrization of a polarizable model was realized.[28,29,129–133] Polarizable dipoles describe the induction effect whereby the electric field caused by other atoms and molecules polarize an atom center, which in turn produces an electric field that affects neighboring centers and their fields.

More recent activity has seen the development of fluctuating charge models,[30–32,34,125,134] which allow for significant shifts of electron density from one atom to surrounding atoms or bonds within the same molecule. The fluctuating charge force fields are based on the electronegativity equalization method originally developed in the context of density functional theory (DFT),[135] where quantum chemical properties such as electronegativity, defined as the negative of the gradient of the electron chemical potential with respect to the electronic density, and hardness, the corresponding second derivative that measures the resistance of an atomic center to lose electron density, are used. Including polarizability in the empirical force field typically adds roughly a factor of 2 additional cost relative to nonpolarizable energy and force evaluations. There still remain important issues in how to allow charge transfer between separate molecules, how to describe polarization anisotropy in fluctuating charge models,[136] computational efficiency in Monte Carlo simulation,[137] and extensions to protein/water simulations.

Higher order effects beyond the polarizable, rigid empirical force fields for the modeling of water include permitting bond lengths and angles to vibrate as in flexible water models[29,138–141] as well as incorporation of quantum effects using either hybrid molecular mechanics/quantum mechanics techniques,[142,143] path integral molecular dynamics,[144–148] or fully quantum treatments of electronic structure,[35–38] all of which provide another interesting point of comparison between experiment and theory. In this review we focus on the promising emerging area of ab initio molecular dynamics simulations (sometimes referred to as CPMD due to the clever Car–Parrinello algorithm),[149] where forces due to the electrons acting on the atoms are calculated on the fly using DFT in a plane wave basis. The cost of these calculations rises as $N^3$, where $N$ is the number of basis functions or plane waves per atom, with a large coefficient relative to classical simulations that make these approaches computationally demanding but potentially more predictive.

An important issue encountered in the simulation of water is how best to evaluate the long-range Coulombic forces. It is now accepted that the best way to account for long-range Coulombic forces is through the Ewald summation,[150–152] although reaction field approaches are also viable. Typical Ewald simulations employ Cartesian boundary conditions where the system is periodically replicated in the three spatial dimensions and divides the long-range Coulombic interactions into a short-range part that is evaluated in real space (as a direct sum over atomic positions) and a long-range part evaluated in reciprocal space. Practical implementations are usually based on particle mesh Ewald method.[152]

Once these prescriptions are defined for what water model, interactions, or simulation methodology are being evaluated, properties or observables are then numerically calculated based on well-defined statistical mechanical relationships during the course of either molecular dynamics or Monte Carlo simulation.[150] Monte Carlo simulations are most naturally formulated in the canonical ensemble, so that radial distribution functions can be obtained at a fixed density and temperature but dynamical properties of the fluid cannot be straightforwardly determined. A dynamical description of how water molecules evolve in time can be determined by solving Newton's equations of motion, which is inherently based on the microcanonical ensemble. New positions and velocities are determined numerically using various finite difference algorithms, and the propagated error in the updated quantities is proportional to the power of the time step. Extended system equations of motion and associated numerical integrators have been developed that allow extensions from microcanonical ensemble dynamics to sampling of states in the canonical ensemble as well as the isothermal–isobaric ensembles.[153–156] The stability of these finite difference numerical integrator algorithms is dependent upon a time step that is commensurate with the fastest time scale in the system, giving rise to time steps on the order of 1–2 fs ($10^{-15}$ s) for the classical simulations of water, while the artificial dynamics of the electronic mass degrees of freedom impose a time step of ~0.05 fs in the case of ab initio molecular dynamics.[149,157]

Properties such as radial distribution functions are easily evaluated in a classical simulation, where the number of water molecules is typically between 500 and 1000 and which are simulated for time scales on the order of a nanosecond and where structural, thermodynamic, and kinetic properties can be straightforwardly evaluated during the simulation run. Ab initio molecular dynamics is currently struggling with problems stemming from the steep cost of the energy and force evaluation and the reduced time step. The combination of finite size effects, inadequately converged statistics given the short simulation time scales feasible, and adversely effected dynamics while holding the temperature fixed using thermostats is difficult for ab initio molecular dynamics at present. Nonetheless, given that ab initio molecular dynamics has only recently emerged in the simulation arena for modeling the condensed phases of water, we do believe that its promise will be fully realized in the coming century.

An additional benefit of simulating a water model is the calculation or analysis of properties not readily reachable by experiment. An important aspect of water structure that is only indirectly described through the pair correlation functions is the local orientational correlations. In principle, one can define spatial distribution functions where both the radial, $r$, and angular coordinates, $\Omega = (\phi, \iota)$, are used to define spatially unfolded pair correlation functions $g_{OH}(r, \Omega)$ and $g_{OO}(r, \Omega)$ to give a more detailed description of local hydrogen bonding in the liquid.[158] The reconstruction of 3D contour plots of the local hydrogen bonding is also being used in the analysis of aqueous solution data.[159]

## 6. Water Structure at Ambient Conditions

Water structure at ambient conditions has been studied by X-ray[63,69,70,160] and neutron scattering[45,48,72,161,162] over the last 30 years. Figure 2a shows a comparison between X-ray scattering intensities of liquid water under ambient conditions by various research groups. The most recent X-ray data taken at the Advanced Light Source (ALS) at Lawrence Berkeley National Laboratory[40,41] are exhibited with error bars and show that there are real differences when comparing to the scattering curves of past X-ray experiments. Figure 2b shows the $g_{OO}(r)$ from the ALS experiment and other $g_{OO}(r)$'s prior to 2000, including Narten's X-ray scattering experiments from 1972,[63] the neutron scattering experiment by Soper and Phillips[163] in 1986, and neutron scattering by Soper, Bruni, and Ricci in 1997.[103] As seen in Figure 2b, the differences between the current synchrotron experiment and earlier determinations of $g_{OO}(r)$ are in the height and sharpness of the first peak as well as a systematic shift in all peak positions to smaller values of $r$.

The recent X-ray result gives a peak height of 2.8. The previously reported X-ray and more recent neutron studies have first peak height values of 2.2. Much of the information determining the *exact* height and shape of this peak is present in the scattering at wave-vectors above 7.0 Å⁻¹. The smaller and broader first peak in $g_{OO}(r)$, reported by the older
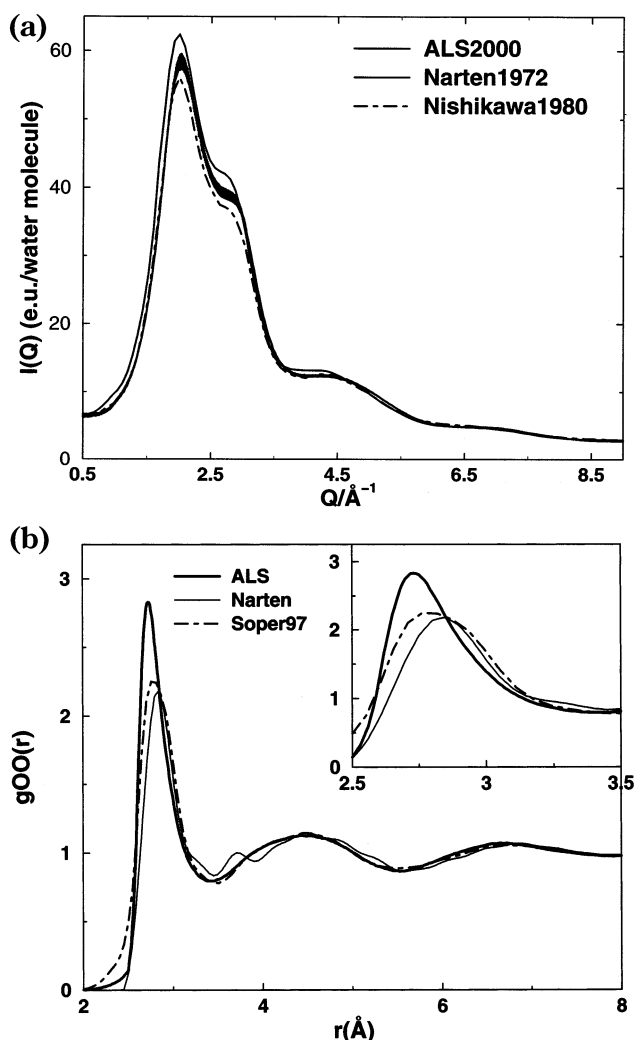


**Figure 2.** Comparison of scattering experimental data on pure water at 25 °C and 1 atm. **(a)** Comparison of X-ray scattering intensities from the ALS[40] (thick solid line), Narten[63] (thin solid line), and Nishikawa[189] (dot−dash line). **(b)** Comparison of experimentally derived $g_{OO}(r)$ data. ALS, X-ray[40] (thick solid line); Narten,[70] X-ray (thin solid line); Soper, Bruni, and Ricci,[103] neutron 1997 (dot−dash line).

X-ray and neutron experiments, manifests itself at higher $Q$ as exponentially damped ripples, decaying much faster than the recent X-ray synchrotron data as seen in Figure 3.

Differences in the height and sharpness of the first peak of $g_{OO}(r)$ result in changes in the coordination number, $N_c$

$$N_c = 4\pi\rho \int_0^{r_{min}} r^2 \, dr \, g_{OO}(r) \qquad (25)$$

where $\rho$ is the number density of water and $r_{min}$ is the location of the first minimum in $g_{OO}(r)$. We find values for $N_c$ of 5.1, 5.2, and 4.7, for Narten and Levy,[63] Soper, Bruni, and Ricci,[103] and the Hura et al. work, respectively. A coordination number below five indicates that liquid water preserves much of its ice-like tetrahedral structuring but with differences in hydrogen-bonding patterns that would also now include deformed or bifurcated hydrogen bonds.[22] We see ~10% reduction in $N_c$ from the X-ray experiment that, together with greater peak heights and posi-
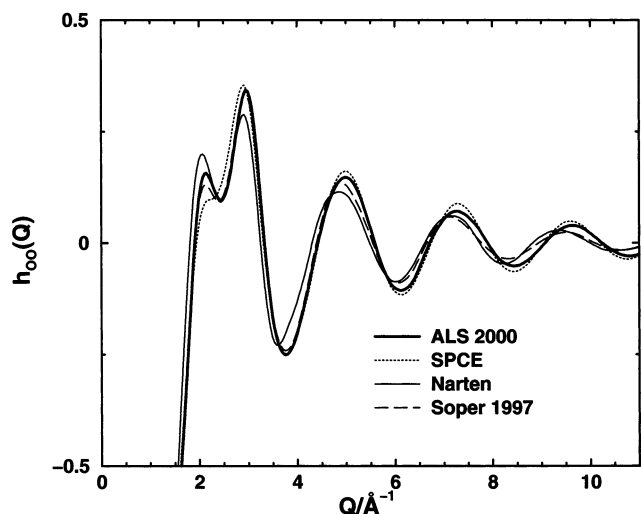
**Figure 3.** $h_{OO}(Q)$ from experiment and simulation. Legend: Narten and Levy[63] (thin solid line); Soper, Bruni, and Ricci[103] (dot−dash line); Hura et al.[40] (thick solid line); SPC/E[24] (dotted line). The curve for Narten and Levy is $H_M(Q)$ taken from their paper;[62] the curve for Soper et al. is taken from applying a Fourier transform to the $g_{OO}(r)$ given in ref 103.

tions shifted to smaller $r$, suggests liquid water is more structured than has been the case based on past scattering studies.

Soper reported new neutron analysis results on previously obtained neutron data using the potential-based reverse Monte Carlo method EPSR[109,116] (Figure 4). The new neutron $g_{OO}(r)$ is in very good agreement with our $g_{OO}(r)$ from X-ray scattering (Figure 4a). In the ESPR analysis used in ref 116, the reference potential is SPC/E, whose $g_{OO}(r)$ agrees well with the X-ray data. This probably helps the better agreement of the new neutron analysis with our X-ray scattering data for $g_{OO}(r)$. Figure 4 parts b and c shows a comparison between (neutron) experimentally derived $g_{OH}(r)$'s and $g_{HH}(r)$'s from 1997 and 2000.[103,116] There is less variation among the data sets for these partial radial distribution functions, especially for $g_{OH}(r)$.

Most water simulation has primarily considered the ambient state. The simulated partial correlation functions of the newer empirical water models such as the nonpolarizable TIP5P model,[27] a rigid polarizable model based on fluctuating charges, TIP4P-pol-1,[31] and a flexible polarizable model based on induced dipoles NCC-vib[29] are shown in Figure 5. Other water models were analyzed in ref 41, and we note that many water models show impressive structural agreement with the recent X-ray experiment.[164] The TIP5P five-site model is particularly noteworthy given its excellent prediction of the ALS $g_{OO}(r)$ data and has produced an accurate fit of densities over a large temperature range.[27] The polarizable models also show very good agreement with $g_{OO}(r)$ and without fitting typically predict the temperature of maximum density. None of the models does an outstanding job in reproducing the reanalyzed neutron scattering $g_{OH}(r)$ and $g_{HH}(r)$ (Figure 5 parts b and c). Whether this is due to continued uncertainty in the experimental data or deficiencies in force fields remains unclear.
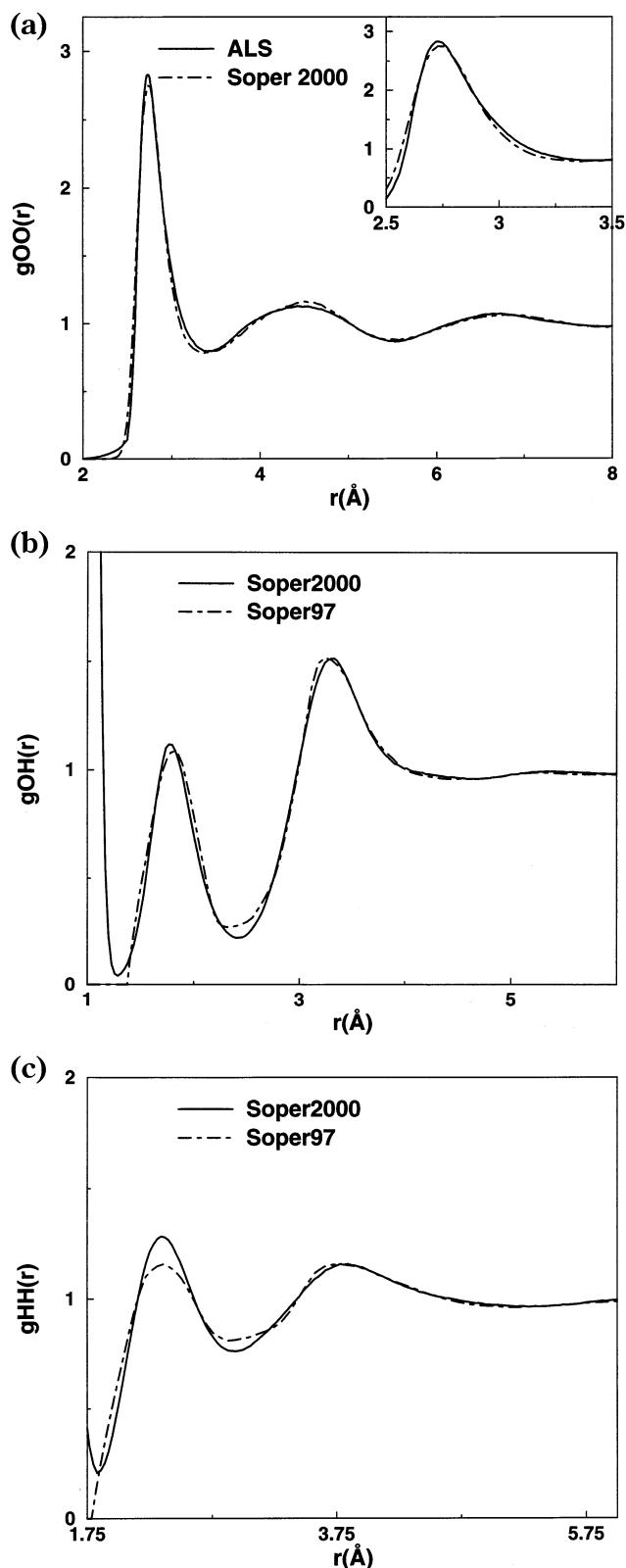


**Figure 4.** Comparison of neutron data on pure water at 25 °C and 1 atm. **(a)** Comparison of ALS X-ray experimental $g_{OO}(r)$[40,41] (solid line) with reanalysis of Soper neutron data, 2000[5] (dashed line). Comparison of neutron data on pure water at 25 °C and 1 atm in 1997[103] (dot−dash line) and 2000[116] (solid line) for **(b)** $g_{OH}(r)$ and **(c)** $g_{HH}(r)$.

Explicit quantum treatments of electronic structure in the condensed phase are an exciting new development in the simulation arena, and a number of ab
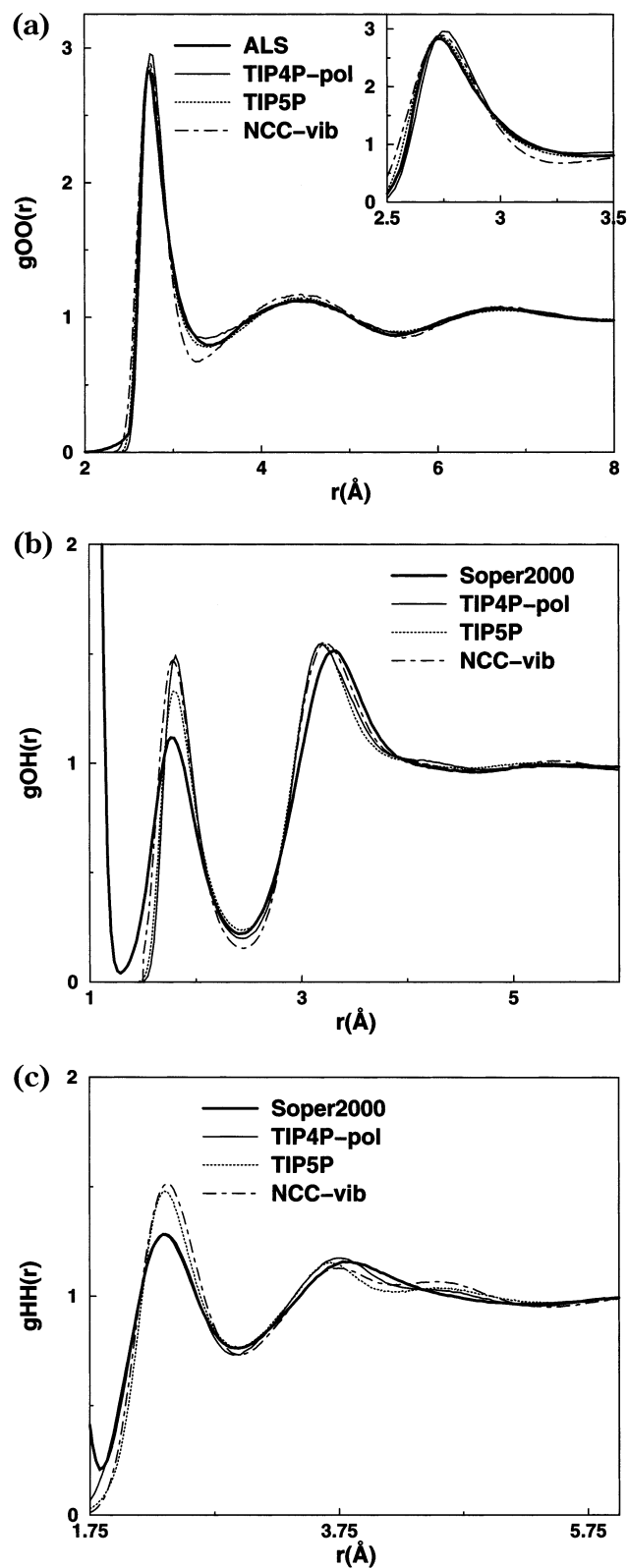
**(a)**



**(b)**



**(c)**



**Figure 5.** Comparison of experimental radial distribution functions (thick solid line) with simulations using empirical force fields for the TIP4P-pol-1[31] (thin solid line), TIP5P[27] (dotted line), and NCC-vib[29] (dot−dash line) models: **(a)** $g_{OO}(r)$, **(b)** $g_{OH}(r)$, and **(c)** $g_{HH}(r)$.

**(a)**



**(b)**



**(c)**



**Figure 6.** Comparison of experimental scattering data with ab initio molecular dynamics simulations. ALS X-ray experimental $g_{OO}(r)$ (thick solid line), ab initio simulation of 10 ps for 64 water molecules, average ionic temperature of 318 K from Silvestrelli and Parrinello[36] (thin solid line), recent ab initio simulation by Schwegler et al.,[187] 3 ps for 54 water molecule average ionic temperature of ∼294 K (dotted line), ab initio simulation of 12 ps for 64 water molecules, average ionic temperature of 307 K from Izvekov and Voth[38] (dot−dash line): **(a)** $g_{OO}(r)$, **(b)** $g_{OH}(r)$, **(c)** $g_{HH}(r)$.

initio aqueous simulations have been reported.[35−38] All have relied on a local density approximation to density functional theory. In Figure 6 we show a comparison of our ALS-derived data with several recently reported ab initio simulated $g_{OO}(r)$'s. The
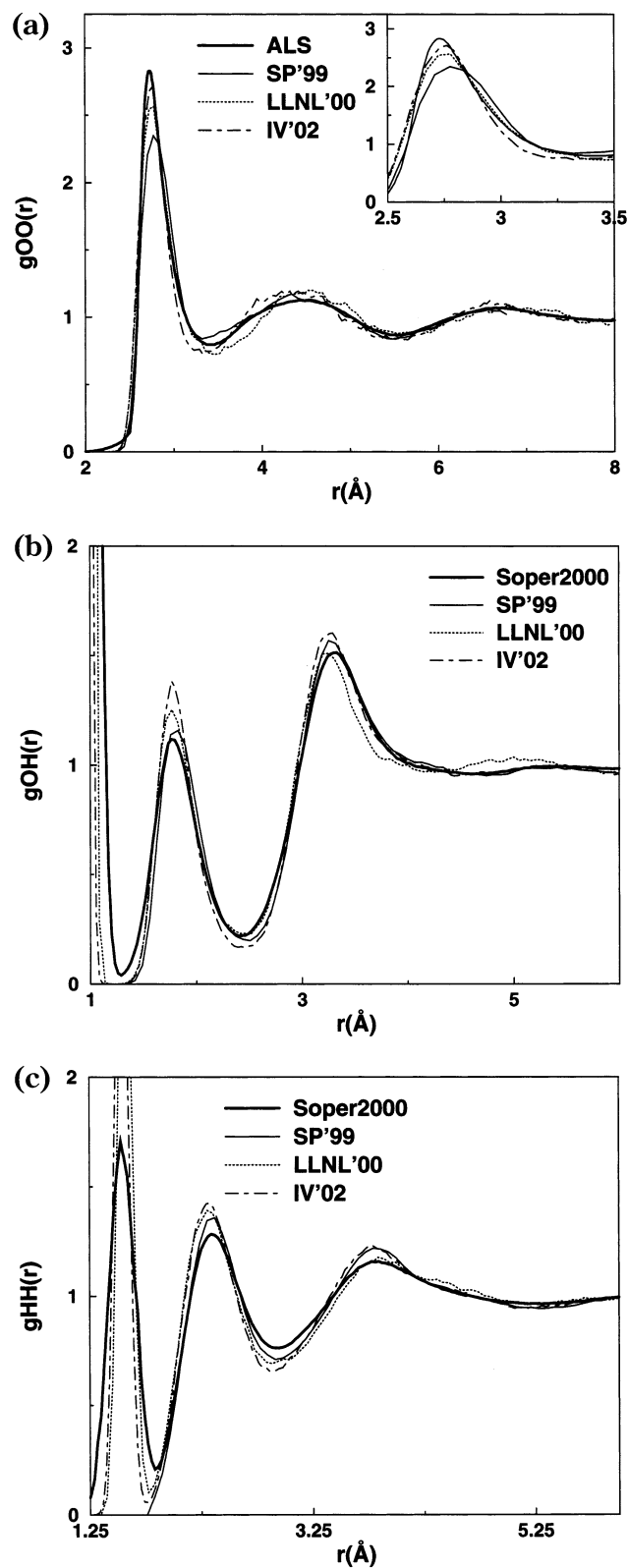
relevant details of the reported ab initio simulations are a 10 ps, 64 water molecule MD run with a gradient-corrected BLYP functional with an average temperature of 318 K,[36] a 6.5 ps, 64 water molecule MD run with a BLYP functional using GGC as the exchange-correlation energy functional with an average temperature of 312 K,[38] and a 6.5 ps, 54 water molecule MD run with the PBE functional and at a temperature of ~305 K.[35]

We found in our previous study that quantitative agreement using ab initio simulation was not as adequate as one would hope, for reasons well understood from classical simulation benchmarks that have overcome dependence on initial conditions, short time scales of simulations, and variation in properties that arise due to differences in temperature,[165] density,[166] or finite size effects.[167,168] However, the current standard of 56−64 water molecules seems sufficient for eliminating the most obvious problems of finite size effects and careful attention to initial conditions seem to have improved the most recent ab initio molecular dynamics simulations. There are still problems in fixing the temperature in ab initio molecular dynamics simulations, presumably because for these small system sizes temperature fluctuations will be large and the Nose−Hoover thermostats will adversely affect the calculated dynamical quantities. Since dynamical observables are just as desirable as the evaluation of structure, the property statistics are collected in the microcanonical ensemble instead.

The assessment of the simulated $g_{OO}(r)$'s show that there is still some differences with experiment, although the more recent simulations now show better agreement in the first peak. Given the agreement between the ab initio simulations and the current experimental $g_{OH}(r)$'s and $g_{HH}(r)$'s from neutron scattering, we conclude that the ab initio simulations reproduce the data very well. Furthermore, it is easy to imagine that if the simulations were able to hold the average temperature to room temperature and then nuclear quantum effects were added that are known to "soften" structure, that quantitative agreement with experiment might soon be realized.[148]

## 7. Water Structure Away from Ambient Conditions

As temperature and pressure are increased or decreased, the structure of the three-dimensional hydrogen-bonded network of water changes relative to the reference ambient temperature liquid. This is manifested in the anomalous properties of liquid water, which become either more pronounced or are reduced to that of a normal liquid, at these temperature and pressure extremes. These altered water properties in turn can expand the functional versatility of the liquid solvent under these new conditions and has important connections to the origin of life in extreme environments, the atmospheric sciences, and the development of new environmentally friendly solvents.

Water under pressure has been characterized by both neutron[71,75,116] and X-ray scattering.[65,66,160,169,170] These structural studies indicate that when water is placed under pressure, the number of hydrogen

bonds per water molecule does not change by any appreciable amount relative to the ambient state, although they are now bent out of their ideal orientation and are correspondingly weaker energetically. The effect of pressure is particularly noticeable in the $g_{OO}(r)$, where the second peak that is a signature of local tetrahedral structure diminishes as pressure is increased. The liquid structure at high pressure is nearly independent of temperature variation.

Water near its critical point ($T_c = 647$ K, $\rho_c = 0.322$ g/mL) is studied for both its practical importance as a clean solvent for industrial chemistry and to address fundamental questions regarding how structural changes in the high-temperature, high-pressure liquid result in a significant decrease in viscosity and a reversal of solubility preferences between hydrophobic and polar solutes relative to ambient conditions. Typically the investigation of supercritical water extends over isochores between 0.05 and 1 g/mL or isotherms between ~473 and 1273 K. As water is heated into sub- and supercritical regimes, the number of hydrogen bonds per water molecule has been shown to decrease. At what temperature would the total breakdown of hydrogen bonding be observed has been debated for many years, with most experimental studies, including Raman,[171] X-ray scattering,[47] and infrared,[172] suggesting that tetrahedral bonding persists to at least ~650 K and possibly up to ~770 K at 100 MPa.[173]

Using the neutron scattering method of isotopic substitution, Postorino et al. reported partial correlation functions at one supercritical state point of $T = 673$ K and $\rho = 0.66$ g/mL and showed the disappearance of the hydrogen-bonding peak in $g_{OH}(r)$.[50,74] This was in contrast to partial correlation functions derived from simulation using popular two-body and polarizable water force fields, which exhibit a persistence of hydrogen bonding to much higher temperatures.[28,50,174,175] This stimulated much debate and constructive interplay between simulation and further experimental studies that eventually and clearly indicated that hydrogen bonding persists to temperatures well beyond the original neutron scattering estimate.[46−49,103,171] There is now consensus that the space-filling percolating hydrogen-bonding network of the liquid (a model proposed by Stanley and Teixeira based upon connectivity concepts from correlated-site percolation theory[176]) present under ambient conditions collapses,[162] although local hydrogen bonding is still present near the critical temperature and density.

Figure 7 shows a comparison of the partial radial distribution functions from X-ray scattering,[169] neutron scattering,[103] and simulations using the TIP4P water model at the subcritical state $T = 573$ K and $\rho = 0.72$ g/mL and supercritical state of $T = 673$ K and $\rho = 0.66$ g/mL (further detail can be found in ref 177). The number of hydrogen bonds is estimated by integration under the first peak of $g_{OH}(r)$, similar to that used in eq 25 for the water coordination number. At ambient conditions $n_{HB} = 3.3$, while at $T = 573$ K and $\rho = 0.72$ g/mL it is now $n_{HB} = 2.4$. Overall the agreement between simulation and experiment is very good for the subcritical thermodynamic point.
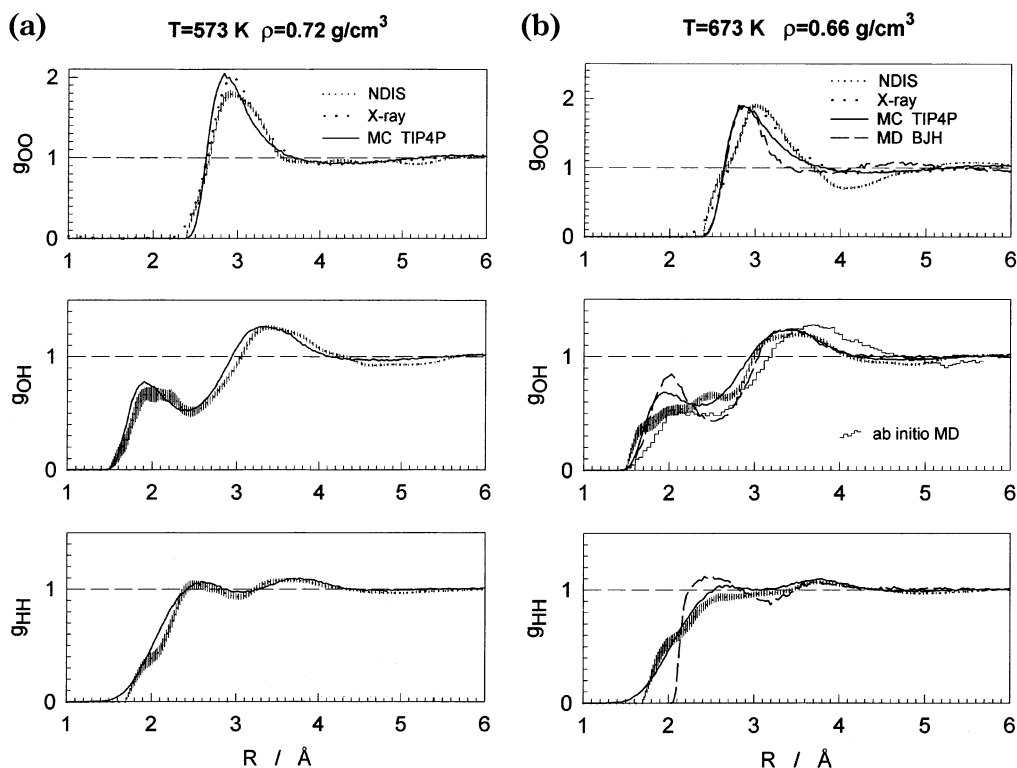
**Figure 7.** Experimental scattering data and simulations for supercritical water at **(a)** $T = 573$ K and $\rho = 0.72$ g/mL for $g_{OO}(r)$ (top), $g_{OH}(r)$ (middle), and $g_{HH}(r)$ (bottom); **(b)** $T = 673$ K and $\rho = 0.66$ g/mL for $g_{OO}(r)$ (top), $g_{OH}(r)$ (middle), and $g_{HH}(r)$ (bottom). (Reprinted with permission from ref 177. Copyright 1997 American Chemical Society.)

The agreement between experiments and between experiment and simulation is not as good at the supercritical state examined in Figure 7b, although $n_{HB}$ is estimated to be 2.1 by all approaches. The corrected neutron data still show a much stronger trend for loss of hydrogen bonding as a function of temperature and density than does simulation.[173,177] A comparison of more recent neutron data[46] and ab initio molecular dynamics simulations[178] (which agree well with each other) do see greater persistence in hydrogen bonding at supercritical conditions as judged by a small first peak in $g_{OH}(r)$.

A current conundrum in simulation of supercritical conditions is the attempt to accurately reproduce both structure and thermodynamic data using one water model or at least some clear consistent improvements using more sophisticated polarizable water models. Overall the two-body potentials are fairly accurate for thermodynamic properties such as densities, isobaric heat capacities, and isothermal compressibility over the range of supercritical temperatures between 573 and 1273 K.[173] However, they appear to be less accurate when it comes to reproducing the available partial correlation functions for water structure from neutron scattering over a range of supercritical conditions.[179] Even though there seems to be a clear trend that polarizable water models better describe structure under supercritical conditions, they are still underperforming when reproducing thermodynamic properties of the phase equilibria envelope.[173,179]

For example, inadequate water structure was reported for a SPC-based polarizable model, the SPC-pol force field, while a TIP4P-pol force field developed in the same group found reasonable structure.[31] By

contrast, the SPC-pol did better than TIP4P-pol in reproducing saturated vapor and liquid densities, the heats of vaporization, and the liquid-phase dielectric constants.[31] It was determined by Errington and Panagiotopoulos that polarizable models based on existing force fields with a SPC or TIP4P geometry, while adequately describing the vapor–liquid coexistence curve, did not provide a satisfactory description of the liquid structure at ambient conditions.[180] The interface between the reference water potential geometry on top of which polarizability is added seems to be important for a consistent water model for structure and for phase equilibrium properties, but there are no clear indicators yet on how to obtain both.

Supercooled water, common in the atmosphere, shows enhanced anomalies in that the coefficient of thermal expansion, isothermal compressibility, and specific heat at constant pressure specific heat appear to diverge at $-46$ °C based on extrapolations of experimental data taken over the range from 0 to $-38$ °C.[8] The supercooled liquid is difficult to study experimentally since the freezing process can be stimulated by the presence of small ice nuclei. Because the nucleation rate of ice nuclei increases with decreasing temperature, experimental studies below $-25$ °C require the use of emulsions that diminish the nucleation event for freezing. Freezing is an insurmountable problem (so far) for characterizing the liquid water structure into the deeply supercooled regime beyond $-38$ °C.

The neutron diffraction studies performed by Bellissent-Funel and co-workers have attempted to establish two structural limits in liquid water over large ranges in temperature and pressure that cor-

respond closely to the low-density and high-density forms of amorphous ice, LDA and HDA.[8,9,75,181,182] Figure 8 shows a composite $g_L(r)$ from LDA and HDA data whose relative weights are fit to an equation of the form

$$g_L(r) = \alpha(T,P)g_L^{LDA}(r) + (1 - \alpha(T,P))g_L^{HDA}(r) \quad (26)$$

These structural experiments and interpretation suggest that the liquid under high temperature and pressure would yield HDA ice when quenched, while the structure of liquid water changes toward the LDA ice structure when the liquid is supercooled at low pressures.

These conclusions have important implications about the overall phase diagram of water and water anomalies.[8] There have been three hypotheses about a unified picture of water and its anomalous behavior: the stability limit hypothesis,[183] the singularity-free hypothesis,[184] and the liquid–liquid phase-transition hypothesis.[185] However, there are severe experimental limitations in accessing the region of the phase diagram that could usefully discriminate among these hypotheses. The role of simulation with regard to pressure and temperature extremes is to "extend" the range of the characterized phase diagram where experiment cannot reach to address broader issues of phenomenology and a unified picture of water.

Often two "structural" extremes of water models such as SPC, which is considered to be understructured, and ST2, which is considered to be overstructured, are used in simulations designed to test these hypothesis.[186] As we have already noted, neither is an accurate model of water structure as compared to other models under ambient conditions; however, it is fair to say that they "bracket" the structural behavior of real water at room temperature and pressure. It has been shown that simulation with both models is useful for reproducing and interpreting the structural data over large ranges of temperature and pressure[44] as well as bracketing other water properties such as the temperature of maximum density line (although it is shifted in the temperature–pressure plane relative to experiment).[186] Figure 9 shows that the trend in the structural behavior of water is comparable between SPC/E and experiment over a large range of temperatures and pressures.[44] In fact, simulations using SPC in the supercooled region determined a second critical point,[185] below which the liquid separates into two distinct liquid phases: a low-density liquid at low pressures and a high-density liquid at high pressure, stimulating further experimental investigations that might prove or disprove the liquid–liquid phase transition hypothesis.[8]

## 8. Conclusion

From a scattering experiment one can (usually) only infer an aspect of the structural properties of the three-dimensional water network through the structure factor and its related radial distribution functions. These are inherently two-body correlations only, although they are indirectly informative about
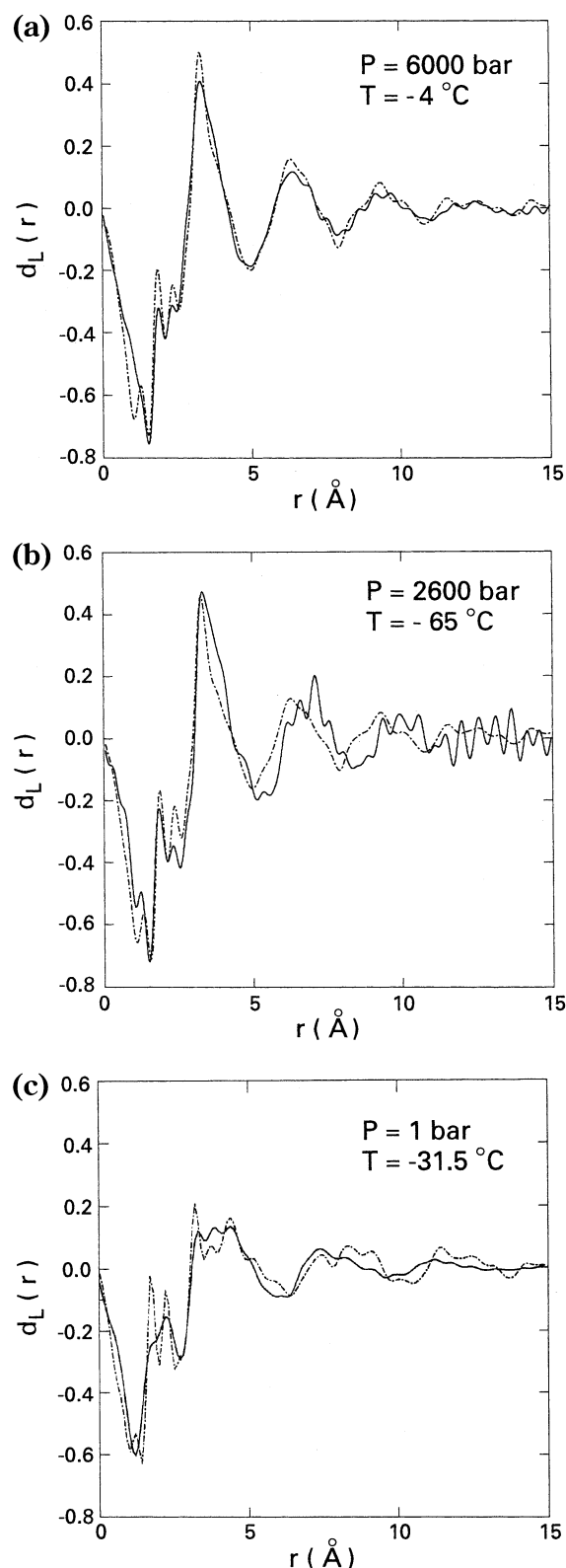


**Figure 8.** Pair correlation function, $g_L(r)$ of three thermodynamic states from experiment (solid line) as compared with the result of the fit using eq 26 (dotted line). At high pressure (top), the structure of the liquid is close to that of high-density amorphous ice near 2600 bar and −65 °C (middle). The fit with the pair correlation function of deeply supercooled water and with that of low-density amorphous ice (bottom) shows that the structure of the liquid phase is dominated by that of low-density amorphous ice.[9] (Reprinted with permission from ref 9. Copyright 1998 Publisher.)
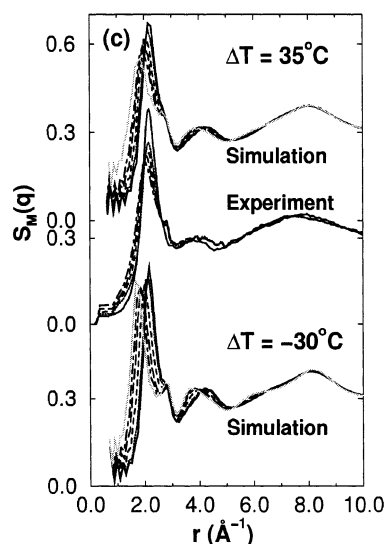
**Figure 9.** Structure factor, $S_M(Q)$, from experiment and SPC/E simulations for supercooled water. The plots show that the trend in the structural behavior of water is comparable between SPC/E and experiment over a large range of temperatures and pressures. (Reprinted with permission from ref 44. Copyright 1999 Publisher.)

the three-dimensional, tetrahedral nature of the hydrogen-bonded network. Furthermore, structure is only one of many properties of water, and other experiments that probe dynamics over many time scales that characterize the thermodynamic phase diagram of water or its properties in solution and in its role as a solvent are vital for full understanding of this most relevant of fluids.

X-ray scattering on water provides us with either a molecular centers distribution function or with careful experiments and theoretical analysis, the partial correlation function, $g_{OO}(r)$. Neutron scattering can provide us with local orientational structure through either a composite pair distribution function, roughly equally weighted between $g_{OH}(r)$ and $g_{HH}(r)$, or an estimate of all three partial correlation functions using isotopic substitution experiments. We have carefully reviewed the scattering techniques of X-ray and neutron scattering, with special attention focused on the inherent difficulty and recent progress made in data analysis in each of these experiments to extract the structural content from the measured intensity.

Overall the experiments have reached a stage where data acquisition with good statistical accuracy is now in hand. However, it is the correction of difficult systematic errors in the data that have made for a history of uncertainty in the reported structural correlation functions. In essence, most of the systematic experimental error corrections are relatively straightforward to account for polarization, absorption, and other geometric corrections relevant to the details of a given scattering experiment. The primary problem in X-ray and neutron scattering is the removal of Compton or inelastic scattering, since only elastic scattering has meaningful structural content. X-ray scattering has benefited from technical advances at synchrotron facilities that allow the accurate measurement of the inelastic cross-section directly, so that we have a very good estimate of

Compton scattering removal for water.[92] The removal of inelastic scattering from neutron data is more difficult by comparison because the measurement is not performed at constant $Q$, but instead the cross-section is measured at constant scattering angle $\theta$. The Placzek corrections account for inelastic scattering using a mass expansion in powers of neutron mass to atomic mass, which converges poorly for low molecular weight compounds such as water, and apparently higher order terms become important at higher temperatures. The problem of correcting for inelasticity was diagnosed as the primary source of error in the original neutron study under supercritical conditions.[103]

At this point in time these very different but complementary experiments have converged on a virtually identical $g_{OO}(r)$ under ambient conditions. The question is whether these experimental measurements using better data analysis are becoming a reliable source of quantitative structural information for water. An optimistic view is that the new X-ray measurements have less uncertainty than previous measurements because they use a state-of-the-art synchrotron source and high-quality CCD detectors, have much better estimates of unwanted Compton scattering, and have more careful theoretical work to restore chemical bonding effects in the weighting of the partial structure factors.[41,57,90,91] Removal of inelastic scattering for neutron scattering remains problematic, but new analysis techniques may be making some headway[116] given the independent confirmation of the neutron $g_{OO}(r)$ by the recent X-ray experiments. We might hope that the recent neutron $g_{OH}(r)$ and $g_{HH}(r)$ partials are also better at ambient conditions since neutron scattering signal from hydrogen correlations is the strongest. However, the long history of experimental uncertainties in X-ray and neutron scattering, which we have attempted to discuss fully in this review, suggest that more time is needed to assess whether these experiments are fully converged.

Even when or if these systematic error corrections are accounted for in the scattering intensity, the inversion of the corrected intensity to determine real-space radial or orientational partial correlation functions remains an additional source of uncertainty. Various techniques have been introduced over the years including $Q$-space continuation, fitting procedures in $r$-space, reverse Monte Carlo methods, and successors of RMC such as the commonly used ESPR approach in neutron scattering. While RMC has been found to be useful in the context of atomic and ionic solutions, it has proven less effective for molecular fluids with strong orientational correlations. The comparison of simulated structure with the more contrived radial distribution functions from diffraction experiments is less than ideal for comparing and analyzing the structural properties of liquid water. Ab initio molecular dynamics provides a means for obtaining X-ray scattering through the electron density directly, avoiding the ambiguities and errors of inversion to real-space functions for comparison.

When we consider the characterization of water structure over the liquid region of the phase diagram,

it is apparent that computer simulation has played an equal, and sometimes pivotal, role in both the quantitative characterization of the water liquid and the advancement of our qualitative understanding of water and its anomalies. For example, the exciting emerging area of ab initio molecular dynamics is beginning to overcome steep computational demands, so that its role as a predictive simulation method is starting to be realized.[38,178,187] In addition, there are three examples of success in theoretical modeling when considering three very different state points of the water liquid.

First, simulation models of water have been better at predicting water structure at ambient conditions for some time. Almost all empirical water models, regardless of the number of charge centers and whether polarizable or nonpolarizable, exhibit a relatively high and sharp first peak in $g_{OO}(r)$, contrary to experiments preceding the year 2000. This is because parametrization of a water model that exhibits sensible dielectric and diffusion constants, pressure, density maximum, and hydrogen-bonded structure, is inconsistent or unattainable with a model that gives a shorter and more broad first peak of the oxygen–oxygen radial distribution function.[188]

Of course, we are interested in water properties beyond ambient conditions, and an obvious question is the impact of simulation for thermodynamic points at which many existing water models are not typically parametrized. There is some disagreement as to how "extensible" water models are to greater extremes in pressure and temperature, but the level of disagreement depends on whether qualitative insight or quantitative modeling is desired.

For example, simulation using relatively simple water force fields played an important part in pointing out inherent problems in the neutron scattering data analysis under supercritical conditions, data which have since been reanalyzed to give better agreement between experiment and simulation. However, because supercritical water has very direct industrial importance and ample available experimental data against which to compare, the primary emphasis for simulation studies at present is to predict accurate thermodynamic and structural data for liquid-phase equilibrium. While well-established empirical two-body force fields do a very reasonable job of reproducing thermodynamic data of phase equilibria far removed from the ambient state. Structure is less adequately reproduced.[173] The current activity in simulation of supercritical water is centered around the next generation of polarizable force fields and much greater emphasis on more accurate and predictive water models for both structure and thermodynamics.

By venturing into parts of the phase diagram that are difficult or impossible to reach experimentally, water simulation has also played a primary role in discovery of phenomena that broadly impacts our understanding of water's anomalous properties and its behavior even at ambient conditions. Simulations using SPC in the supercooled region found evidence for a second critical point,[185] not yet confirmed experimentally, below which it is hypothesized that the liquid separates into two distinct liquid phases: a low-density liquid at low pressures and a high-density liquid at high pressure. It has been argued that two simulations using two different water models with different structural signatures (such as SPC and ST2) can bracket the behavior of real water, and in fact, the subsequent ST2 simulation provided further evidentiary support for a liquid–liquid phase transition.[186] These simulations have driven much of the experimental investigations that might prove or disprove the current competing theories of a unified picture of water such as that discussed in ref 8.

Structural measurements, whether they are derived from experiment or simulation, play a dominant role in our thinking about the hydrogen-bonded network of water and its connection to thermodynamics and kinetics across the phase diagram. In this review we considered water structure from the viewpoint of X-ray and neutron scattering measurements and computer simulation, whose complementary strengths have together provided a balanced but still only partially revealed truth as to the nature of the topology of the hydrogen-bonded network.

## 9. Acknowledgments

## 10. References

(1) *Water, a comprehensive treatise*; Franks, F., Ed.; Plenum Press: New York, 1972.
(2) Dore, J. C.; Teixeira, J. *Hydrogen-bonded liquids: proceedings of the NATO Advanced Study Institute on Hydrogen-bonded Liquids,* Institut Scientifique de Cargèse, Corsica, April 3–15, 1989; Kluwer Academic Publishers: Dordrecht,; Boston, 1991.
(3) Bellissent-Funel, M. C.; Dore, J. C. *Hydrogen bond networks*; Kluwer Academic Publishers: Dordrecht, Boston, 1994.
(4) Franks, F. *Water: a matrix of life*, 2nd ed.; Royal Society of Chemistry: Cambridge, 2000.
(5) Stillinger, F. H. *Science (USA)* **1980**, *209*, 451–7.
(6) Robinson, G. W. *Water in biology, chemistry, and physics: experimental overviews and computational methodologies*; World Scientific: Singapore; River Edge, NJ, 1996.
(7) Ball, P. *Life's matrix: a biography of water*; 1st ed.; Farrar Straus and Giroux: New York, 2000.
(8) Mishima, O.; Stanley, H. E. *Nature* **1998**, *396*, 329–335.
(9) Bellissent-Funel, M. C. *Nuovo Cimento Soc. Ital. Fis. D* **1998**, *20*, 2107–2122.
(10) Ding, K.; Chandler, D.; Smithline, S. J.; Haymet, A. D. J. *Phys. Rev. Lett.* **1987**, *59*, 1698–701.
(11) Headgordon, T.; Stillinger, F. H. *J. Chem. Phys.* **1993**, *98*, 3313–3327.
(12) Lazaridis, T.; Paulaitis, M. E. *J. Phys. Chem.* **1992**, *96*, 3847–3855.
(13) Hummer, G.; Garde, S.; Garcia, A. E.; Paulaitis, M. E.; Pratt, L. R. *J. Phys. Chem. B* **1998**, *102*, 10469–10482.

(14) Pratt, L. R.; Chandler, D. *J. Chem. Phys.* **1977**, *67*, 3683−704.

(15) Headgordon, T. *J. Am. Chem. Soc.* **1995**, *117*, 501−507.

(16) Stillinger, F. H.; Rahman, A. *J. Chem. Phys.* **1974**, *60*, 1545−57.

(17) Lazaridis, T.; Karplus, M. *J. Chem. Phys.* **1996**, *105*, 4294−4316.

(18) Matubayasi, N.; Gallicchio, E.; Levy, R. M. *J. Chem. Phys.* **1998**, *109*, 4864−4872.

(19) Luzar, A. *Chem. Phys.* **2000**, *258*, 267−276.

(20) Luzar, A.; Chandler, D. *Nature* **1996**, *379*, 55−57.

(21) Starr, F. W.; Harrington, S.; Sciortino, F.; Stanley, H. E. *Phys. Rev. Lett.* **1999**, *82*, 3629−3632.

(22) Rahman, A.; Stillinger, F. H. *J. Am. Chem. Soc.* **1973**, *95*, 7943−8.

(23) Sorenson, J. M.; Hura, G.; Soper, A. K.; Pertsemlidis, A.; Head-Gordon, T. *J. Phys. Chem. B* **1999**, *103*, 5413−5426.

(24) Berendsen, H.; Postma, J.; van Gunsteren, W. F.; Hermans, J. In *Intermolecular forces: proceedings of the Fourteenth Jerusalem Symposium on Quantum Chemistry and Biochemistry*; Pullman, B., Ed.; D. Reidel. Sold and distributed in the U.S.A. and Canada by Kluwer: Boston, Dordrecht, 1981; Vol. 14.

(25) Berendsen, H. J. C.; Grigera, J. R.; Straatsma, T. P. *J. Phys. Chem.* **1987**, *91*, 6269−71.

(26) Jorgensen, W. L.; Chandrasekhar, J.; Madura, J. D.; Impey, R. W.; Klein, M. L. *J. Chem. Phys.* **1983**, *79*, 926−35.

(27) Mahoney, M. W.; Jorgensen, W. L. *J. Chem. Phys.* **2000**, *112*, 8910−8922.

(28) Chialvo, A. A.; Cummings, P. T. *J. Chem. Phys.* **1996**, *105*, 8274−8281.

(29) Corongiu, G.; Clementi, E. *J. Chem. Phys.* **1992**, *97*, 2030−2038.

(30) Svishchev, I. M.; Kusalik, P. G.; Wang, J.; Boyd, R. J. *J. Chem. Phys.* **1996**, *105*, 4742−4750.

(31) Chen, B.; Xing, J. H.; Siepmann, J. I. *J. Phys. Chem. B* **2000**, *104*, 2391−2401.

(32) Wallqvist, A.; Berne, B. J. *J. Phys. Chem.* **1993**, *97*, 13841−51.

(33) van der Spoel, D.; van Maaren, P. J.; Berendsen, H. J. C. *J. Chem. Phys.* **1998**, *108*, 10220−10230.

(34) Liu, Y. P.; Kim, K.; Berne, B. J.; Friesner, R. A.; Rick, S. W. *J. Chem. Phys.* **1998**, *108*, 4739−4755.

(35) Schwegler, E.; Galli, G.; Gygi, F. *Phys. Rev. Lett.* **2000**, *84*, 2429−2432.

(36) Silvestrelli, P. L.; Parrinello, M. *J. Chem. Phys.* **1999**, *111*, 3572−3580.

(37) Sprik, M.; Hutter, J.; Parrinello, M. *J. Chem. Phys.* **1996**, *105*, 1142−1152.

(38) Izvekov, S.; Voth, G. A. *J. Chem. Phys.* **2002**, in press.

(39) Karnicky, J. F.; Pings, C. J. In *Advances in Chemical Physics*; Prigogine, I., Rice, S. A., Eds.; Wiley: New York, 1976; Vol. 34.

(40) Hura, G.; Sorenson, J. M.; Glaeser, R. M.; Head-Gordon, T. *J. Chem. Phys.* **2000**, *113*, 9140−9148.

(41) Sorenson, J. M.; Hura, G.; Glaeser, R. M.; Head-Gordon, T. *J. Chem. Phys.* **2000**, *113*, 9149−9161.

(42) Bosio, L.; Teixeira, J.; Dore, J. C.; Steytler, D. C.; Chieux, P. *Mol. Phys.* **1983**, *50*, 733−40.

(43) Bellissentfunel, M. C.; Teixeira, J.; Bosio, L.; Dore, J. C. *J. Phys.-Condens. Matter.* **1989**, *1*, 7123−7129.

(44) Starr, F. W.; Bellissent-Funel, M. C.; Stanley, H. E. *Phys. Rev. E* **1999**, *60*, 1084−1087.

(45) Dore, J. C.; Sufi, M. A. M.; Bellissent-Funel, M. C. *Phys. Chem. Chem. Phys.* **2000**, *2*, 1599−1602.

(46) Bellissent-Funel, M. C. *J. Mol. Liq.* **2001**, *90*, 313−322.

(47) Gorbaty, Y. E.; Kalinichev, A. G. *J. Phys. Chem.* **1995**, *99*, 5336−5340.

(48) Nakahara, M.; Matubayasi, N.; Wakai, C.; Tsujino, Y. *J. Mol. Liq.* **2001**, *90*, 75−83.

(49) Ohtaki, H.; Radnai, T.; Yamaguchi, T. *Chem. Soc. Rev.* **1997**, *26*, 41−51.

(50) Postorino, P.; Tromp, R. H.; Ricci, M. A.; Soper, A. K.; Neilson, G. W. *Nature* **1993**, *366*, 668−670.

(51) Dore, J. *Chem. Phys.* **2000**, *258*, 327−347.

(52) Enderby, J. E.; Howells, W. S.; Howe, R. A. *Chem. Phys. Lett. (Netherlands)* **1973**, *21*, 109−12.

(53) Enderby, J. E. *Proc. R. Soc. London A, Math. Phys. Sci. (UK)* **1975**, *345*, 107−117.

(54) Luzar, A.; Soper, A. K.; Chandler, D. *J. Chem. Phys.* **1993**, *99*, 6836−6847.

(55) Finney, J. L.; Soper, A. K. *Chem. Soc. Rev.* **1994**, *23*, 1−10.

(56) Finney, J. L. *Faraday Discuss.* **1996**, 1−18.

(57) Neuefeind, J.; Zeidler, M. D.; Poulsen, H. F. *Mol. Phys.* **1996**, *87*, 189−201.

(58) Soper, A. K. *J. Phys.-Condens. Matter.* **1997**, *9*, 2717−2730.

(59) Hura, G.; Sorenson, J. M.; Glaeser, R. M.; Head-Gordon, T. *Perspect. Drug Discovery Des.* **1999**, *17*, 97−118.

(60) Dubochet, J.; Lepault, J.; Freeman, R.; Berriman, J. A.; Homo, J. C. *J. Microsc. (UK)* **1982**, *128 pt.3*, 219−37.

(61) Morgan, J.; Warren, B. E. *J. Chem. Phys.* **1938**, *6*, 666.

(62) Narten, A. H.; Levy, H. A. *J. Chem. Phys.* **1971**, *55*, 2263−9.

(63) Narten, A. H.; Levy, H. A. In *Water A Comprehensive Treatise*; Franks, F., Ed.; Plenum Press: New York, 1972; Vol. 1.

(64) Blum, L. In *Water, A comprehensive treatise*; Franks, F., Ed.; Plenum Press: New York, 1976; Vol. 3.

(65) Gorbaty, Y. E.; Demianets, Y. N. *Mol. Phys.* **1985**, *55*, 571−88.

(66) Okhulkov, A. V.; Demianets, Y. N.; Gorbaty, Y. E. *J. Chem. Phys.* **1994**, *100*, 1578−1588.

(67) Takeuchi, H.; Nakagawa, M.; Saito, T.; Egawa, T.; Tanaka, K.; Konaka, S. *Int. J. Quantum Chem.* **1994**, *52*, 1339−1348.

(68) Radnai, T.; Ohtaki, H. *Mol. Phys.* **1996**, *87*, 103−121.

(69) Page, D. I. In *Water, a comprehensive treatise*; Franks, F., Ed.; Plenum Press: New York, 1972.

(70) Narten, A. H.; Thiessen, W. E. *Science (USA)* **1982**, *217*, 1033−4.

(71) Neilson, G. W.; Cummings, S. *Conference Proceedings of Workshop on Sample Environments in Neutron and X-ray Experiments*, Grenoble, France, Feb 13−15, 1983; pp 803−5.

(72) Dore, J. C. *J. Mol. Struct.* **1991**, *250*, 193−211.

(73) Soper, A. K.; Turner, J. *Int. J. Mod. Phys. B* **1993**, *7*, 3049−3076.

(74) Postorino, P.; Ricci, M. A.; Soper, A. K. *J. Chem. Phys.* **1994**, *101*, 4123−4132.

(75) Bellissentfunel, M. C.; Bosio, L. *J. Chem. Phys.* **1995**, *102*, 3727−3735.

(76) Egelstaff, P. A. *An introduction to the liquid state*, 2nd ed.; Oxford University Press: Oxford, New York, 1994.

(77) Woolfson, M. M. *An introduction to X-ray crystallography*, 2nd ed.; Cambridge University Press: Cambridge, 1997.

(78) Coppens, P.; Guru Row: T. N.; Leung, P.; Stevens, E. D.; Becker, P. J.; Yang, Y. W. *Conference Proceedings of Ewald Dynamical Diffraction Symposium*, Norman, Oklahoma, 1979; pp 63−72.

(79) King, S. M. In *Modern techniques for polymer characterisation*; Pethrick, R. A., Dawkins, J. V., Eds.; J. Wiley: New York, 1999.

(80) King, S. M. In *Modern Techniques for Polymer Characterization*; Pethrick, R. A., Dawkins, J. V., Eds.; Wiley: New York, 1999.

(81) Windsor, C. G. *Pulsed neutron scattering*; Taylor & Francis, Halsted Press: London, New York, 1981.

(82) *X-ray Storage-Phosphor Imaging-Plate Detectors: High-Sensitivity X-ray Area Detectors*; Amemiya, Y., Ed.; Methods of Enzymology; Academic Press: San Diego, 1997; Vol. 276.

(83) Reference deleted on revision.

(84) *Charge-Coupled Device-Based Area Detectors*; Westbrook, E. M., Naday, I., Eds., 1997; Vol. 276.

(85) Soper, A. K.; Howells, W. S.; Hannon, A. C.; Turner, J. Z.; Bowron, D. T. *ATLAS: Analysis of time-of-flight diffractometer data from liquid and amorphous samples*; CLRC Isis Facility, Rutherford-Appleton Laboratory: United Kingdom, 2000.

(86) Jackson, J. D. *Classical electrodynamics*, 3rd ed.; Wiley: New York, 1999.

(87) Dwiggins, C. W., Jr.; Park, D. A. *Acta Crystallogr., Sect. A: Cryst. Phys. Diffr. Theor. Gen. Crystallogr.* **1971**, *27* (3), 264−72.

(88) Compton, A. H. *Phys. Rev.* **1923**, *21*, 483.

(89) Tavard, C.; Nicolas, D.; Rouault, M. *J. Chim. Phys.* **1967**, *64*, 540.

(90) Wang, J. H.; Tripathi, A. N.; Smith, V. H. *J. Chem. Phys.* **1994**, *101*, 4842−4854.

(91) Watanabe, N.; Ten-no, S.; Pal, S.; Iwata, S.; Udagawa, Y. *J. Chem. Phys.* **1999**, *111*, 827−832.

(92) Watanabe, N.; Hayashi, H.; Udagawa, Y.; TenNo, S.; Iwata, S. *J. Chem. Phys.* **1998**, *108*, 4545−4553.

(93) Guinier, A. *X-ray diffraction in crystals, imperfect crystals, and amorphous bodies*; W. H. Freeman: San Francisco, 1963.

(94) Moccia, R. *J. Chem. Phys.* **1964**, *40*, 2186.

(95) Blum, L. *J. Comput. Phys.* **1971**, *7*, 592−602.

(96) Clough, S. A.; Beers, Y.; Klein, G. P.; Rothman, L. S. *J. Chem. Phys.* **1973**, *59*, 2254−9.

(97) Coppens, P. *X-ray charge densities and chemical bonding*; International Union of Crystallography. Oxford University Press: New York, 1997.

(98) Hansen, N. K.; Coppens, P. *Acta Crystallogr., Sect. A: Cryst. Phys. Diffr. Theor. Gen. Crystallogr.* **1978**, *34* (6), 909−21.

(99) Chang, S.; Head-Gordon, T.; Glaeser, R. M.; Downing, K. H. *Acta Crystallogr., Sect. A* **1999**, *55*, 305−313.

(100) Zhong, S. J.; Dadarlat, V.; Head-Gordon, T.; Glaeser, R. M.; Downing, K. H. *Acta Crystallogr.* Sect. A, **2002**, *58*, 162−170.

(101) Hove, L. V. *Phys. Rev.* **1954**, *95*, 249−262.

(102) Soper, A. K. *J. Phys.-Condens. Matter.* **1996**, *8*, 9263−9267.

(103) Soper, A. K.; Bruni, F.; Ricci, M. A. *J. Chem. Phys.* **1997**, *106*, 247−254.

(104) Soper, A. K.; Silver, R. N. *Phys. Rev. Lett.* **1982**, *49*, 471−4.

(105) Zetterstrom, P.; Soper, A. K.; Schofield, P. *Phys. B* **1997**, *234*, 337−339.

(106) Placzek, G. *Phys. Rev.* **1952**, *86*, 377-.

(107) Zetterstrom, P.; Soper, A. K.; Schofield, P. *Mol. Phys.* **1996**, *88*, 1621−1634.

(108) Soper, A. K.; Luzar, A. *J. Chem. Phys.* **1992**, *97*, 1320−1331.

(109) Soper, A. K. *Chem. Phys.* **1996**, *202*, 295−306.

(110) Bellissentfunel, M. C.; Bosio, L.; Teixeira, J. *J. Phys.-Condens. Matter.* **1991**, *3*, 4065−4074.

(111) Krogh-Moe, J. *Acta Crystallogr.* **1956**, *9*, 951.

(112) Norman, N. *Acta Crystallogr.* **1957**, *10*, 370.

(113) Narten, A. H.; Venkatesh, C. G.; Rice, S. A. *J. Chem. Phys.* **1976**, *64*, 1106−21.
(114) McGreevy, R. L. *Nucl. Instrum. Methods Phys. Res., Sect. A* **1995**, *354*, 1−16.
(115) McGreevy, R. L.; Puszati, L. *Mol. Simul.* **1988**, *1*, 359.
(116) Soper, A. K. *Chem. Phys.* **2000**, *258*, 121−137.
(117) Wallqvist, A.; Mountain, R. D. In *Reviews in Computational Chemistry*; Lipkowitz, K. B., Boyd, D. B., Eds.; Wiley-VCH: New York, 1999; Vol. 13.
(118) Chialvo, A. A.; Cummings, P. T. *Adv. Chem. Phys.* **1999**, *109*, 115−205.
(119) Cornell, W. D.; Cieplak, P.; Bayly, C. I.; Gould, I. R.; Merz, K. M.; Ferguson, D. M.; Spellmeyer, D. C.; Fox, T.; Caldwell, J. W.; Kollman, P. A. *J. Am. Chem. Soc.* **1995**, *117*, 5179−5197.
(120) MacKerell, A. D.; Bashford, D.; Bellott, M.; Dunbrack, R. L.; Evanseck, J. D.; Field, M. J.; Fischer, S.; Gao, J.; Guo, H.; Ha, S.; JosephMcCarthy, D.; Kuchnir, L.; Kuczera, K.; Lau, F. T. K.; Mattos, C.; Michnick, S.; Ngo, T.; Nguyen, D. T.; Prodhom, B.; Reiher, W. E.; Roux, B.; Schlenkrich, M.; Smith, J. C.; Stote, R.; Straub, J.; Watanabe, M.; WiorkiewiczKuczera, J.; Yin, D.; Karplus, M. *J. Phys. Chem. B* **1998**, *102*, 3586−3616.
(121) Stillinger, F. H.; David, C. W. *J. Chem. Phys.* **1978**, *69*, 1473−84.
(122) Barnes, P.; Finney, J. L.; Nicholas, N. D.; Quinn, J. E. *Nature* **1979**, *282*, 459−64.
(123) Lybrand, T. P.; Kollman, P. A. *J. Chem. Phys.* **1985**, *83*, 2923−33.
(124) Chang, T. M.; Dang, L. X. *J. Chem. Phys.* **1996**, *104*, 6772−6783.
(125) Rick, S. W.; Stuart, S. J.; Berne, B. J. *J. Chem. Phys.* **1994**, *101*, 6141−6156.
(126) Halgren, T. A.; Damm, W. *Curr. Opin. Struct. Biol.* **2001**, *11*, 236−242.
(127) Rullmann, J. A. C.; Duijnen, P. T. V. *Mol. Phys.* **1988**, *63*, 451−75.
(128) Sprik, M.; Klein, M. L. *J. Chem. Phys.* **1988**, *89*, 7556−60.
(129) Ahlstrom, P.; Wallqvist, A.; Engstrom, S.; Jonsson, B. *Mol. Phys.* **1989**, *68*, 563−81.
(130) Dang, L. X. *J. Chem. Phys.* **1992**, *97*, 2659−2660.
(131) Bernardo, D. N.; Ding, Y. B.; Kroghjespersen, K.; Levy, R. M. *J. Phys. Chem.* **1994**, *98*, 4180−4187.
(132) Caldwell, J. W.; Kollman, P. A. *J. Phys. Chem.* **1995**, *99*, 6208−6219.
(133) Brodholt, J.; Sampoli, M.; Vallauri, R. *Mol. Phys.* **1995**, *86*, 149−158.
(134) Stern, H. A.; Rittner, F.; Berne, B. J.; Friesner, R. A. *J. Chem. Phys.* **2001**, *115*, 2237−2251.
(135) Parr, R. G.; Donnelly, R. A.; Levy, M.; Palke, W. E. *J. Chem. Phys.* **1978**, *68*, 3801−7.
(136) Rick, S. W. *J. Chem. Phys.* **2001**, *114*, 2276−2283.
(137) Mahoney, M. W.; Jorgensen, W. L. *J. Chem. Phys.* **2001**, *114*, 9337−9349.
(138) Toukan, K.; Rahman, A. *Phys. Rev. B, Condens. Matter* **1985**, *31*, 2643−8.
(139) Dang, L. X.; Pettitt, B. M. *J. Phys. Chem.* **1987**, *91*, 3349−54.
(140) Zhu, S. B.; Yao, S.; Zhu, J. B.; Singh, S.; Robinson, G. W. *J. Phys. Chem.* **1991**, *95*, 6211−6217.
(141) Watanabe, K.; Klein, M. L. *Chem. Phys.* **1989**, *131*, 157−67.
(142) Field, M. J. *Mol. Phys.* **1997**, *91*, 835−845.
(143) Lefohn, A. E.; Ovchinnikov, M.; Voth, G. A. *J. Phys. Chem. B* **2001**, *105*, 6628−6637.
(144) Kuharski, R. A.; Rossky, P. J. *Chem. Phys. Lett.* **1984**, *103*, 357−62.
(145) Delbuono, G. S.; Rossky, P. J.; Schnitker, J. *J. Chem. Phys.* **1991**, *95*, 3728−3737.
(146) Lobaugh, J.; Voth, G. A. *J. Chem. Phys.* **1997**, *106*, 2400−2410.
(147) Guillot, B.; Guissani, Y. *J. Chem. Phys.* **1998**, *108*, 10162−10174.
(148) Stern, H. A.; Berne, B. J. *J. Chem. Phys.* **2001**, *115*, 7622−7628.
(149) Car, R.; Parrinello, M. *Phys. Rev. Lett.* **1985**, *55*, 2471−4.
(150) Allen, M. P.; Tildesley, D. J. *Computer simulation of liquids*; Clarendon Press and Oxford University Press: New York, 1989.
(151) York, D. M.; Darden, T. A.; Pedersen, L. G. *J. Chem. Phys.* **1993**, *99*, 8345−8348.

(152) Darden, T.; Perera, L.; Li, L. P.; Pedersen, L. *Struct. Fold. Des.* **1999**, *7*, R55−R60.
(153) Andersen, H. C. *J. Chem. Phys.* **1980**, *72*, 2384−93.
(154) Martyna, G. J.; Tobias, D. J.; Klein, M. L. *J. Chem. Phys.* **1994**, *101*, 4177−4189.
(155) Tuckerman, M. E.; Parrinello, M. *J. Chem. Phys.* **1994**, *101*, 1302−1315.
(156) Tuckerman, M. E.; Martyna, G. J. *J. Phys. Chem. B* **2001**, *105*, 7598.
(157) Marx, D.; Hutter, J. In *Modern methods and algorithms in Quantum Chemistry*; Grotendorst, J., Ed.; John von Neumann Institute for Computing: Juelich, 2000; Vol. 1.
(158) Svishchev, I. M.; Kusalik, P. G. *J. Chem. Phys.* **1993**, *99*, 3049−3058.
(159) Svishchev, I. M.; Kusalik, P. G. *J. Chem. Phys.* **1994**, *100*, 5165−5171.
(160) Yamanaka, K.; Yamaguchi, T.; Wakita, H. *J. Chem. Phys.* **1994**, *101*, 9830−9836.
(161) Dore, J. C.; Blakey, D. M. *J. Mol. Liq.* **1995**, *65−6*, 85−90.
(162) Jedlovszky, P.; Brodholt, J. P.; Bruni, F.; Ricci, M. A.; Soper, A. K.; Vallauri, R. *J. Chem. Phys.* **1998**, *108*, 8528−8540.
(163) Soper, A. K.; Phillips, M. G. *Chem. Phys.* **1986**, *107*, 47−60.
(164) Burnham, C. J.; Xantheas, S. S. *J. Chem. Phys.* **2002**, *116*, 1500−1510.
(165) Baez, L. A.; Clancy, P. *J. Chem. Phys.* **1994**, *101*, 9837−9840.
(166) Parker, M. E.; Heyes, D. M. *J. Chem. Phys.* **1998**, *108*, 9039−9049.
(167) Denton, A. R.; Egelstaff, P. A. *Z. Phys. B−Condens. Matter* **1997**, *103*, 343−349.
(168) Pratt, L. R.; Haan, S. W. *J. Chem. Phys.* **1981**, *74*, 1864−72.
(169) Gorbaty, Y. E.; Demianets, Y. N. *Chem. Phys. Lett.* **1983**, *100*, 450−4.
(170) Gorbaty, Y. E.; Okhulkov, A. V. *Rev. Sci. Instrum.* **1994**, *65*, 2195−2198.
(171) Walrafen, G. E.; Yang, W. H.; Chu, Y. C. *J. Phys. Chem. B* **1999**, *103*, 1332−1338.
(172) Bondarenko, G. V.; Gorbaty, Y. E. *Dokl. Phys. Chem.* **1973**, *210*, 369−371.
(173) Kalinichev, A. G. In *Reviews in Mineralogy and Geochemistry*; Kubicki, J. D., Cygan, R. T., Ed., 2001; Vol. 42.
(174) Chialvo, A. A.; Cummings, P. T. *J. Chem. Phys.* **1994**, *101*, 4466−4469.
(175) Mountain, R. D. *J. Chem. Phys.* **1995**, *103*, 3084−3090.
(176) Stanley, H. E.; Teixeira, J. *J. Chem. Phys.* **1980**, *73*, 3404−22.
(177) Kalinichev, A. G.; Bass, J. D. *J. Phys. Chem. A* **1997**, *101*, 9720−9727.
(178) Boero, M.; Terakura, K.; Ikeshoji, T.; Liew, C. C.; Parrinello, M. *J. Chem. Phys.* **2001**, *115*, 2219−2227.
(179) Chialvo, A. A.; Yezdimer, E.; Driesner, T.; Cummings, P. T.; Simonson, J. M. *Chem. Phys.* **2000**, *258*, 109−120.
(180) Errington, J. R.; Panagiotopoulos, A. Z. *J. Phys. Chem. B* **1998**, *102*, 7470−7475.
(181) Mishima, O.; Calvert, L. D.; Whalley, E. *Nature* **1984**, *310*, 393−5.
(182) Mishima, O.; Calvert, L. D.; Whalley, E. *Nature* **1985**, *314*, 76−8.
(183) Speedy, R. J.; Angell, C. A. *J. Chem. Phys.* **1976**, *65*, 851−8.
(184) Sastry, S.; Debenedetti, P. G.; Sciortino, F.; Stanley, H. E. *Phys. Rev. E* **1996**, *53*, 6144−6154.
(185) Poole, P. H.; Sciortino, F.; Essmann, U.; Stanley, H. E. *Nature* **1992**, *360*, 324−328.
(186) Harrington, S.; Zhang, R.; Poole, P. H.; Sciortino, F.; Stanley, H. E. *Phys. Rev. Lett.* **1997**, *78*, 2409−2412.
(187) Schwegler, E.; Galli, G.; Gygi, F.; Hood, R. Q. *Phys. Rev. Lett.* **2001**, *8726*, 5501, U38−U40.
(188) Stillinger, F. H. Private communication.
(189) Nishikawa, K.; Kitagawa, K. *Bull. Chem. Soc. Jpn.* **1980**, *63*, 2804.

CR0006831